Cell Reports

Resource

Synthetic Biology Platform for Sensing and Integrating Endogenous Transcriptional Inputs in Mammalian Cells

Graphical Abstract

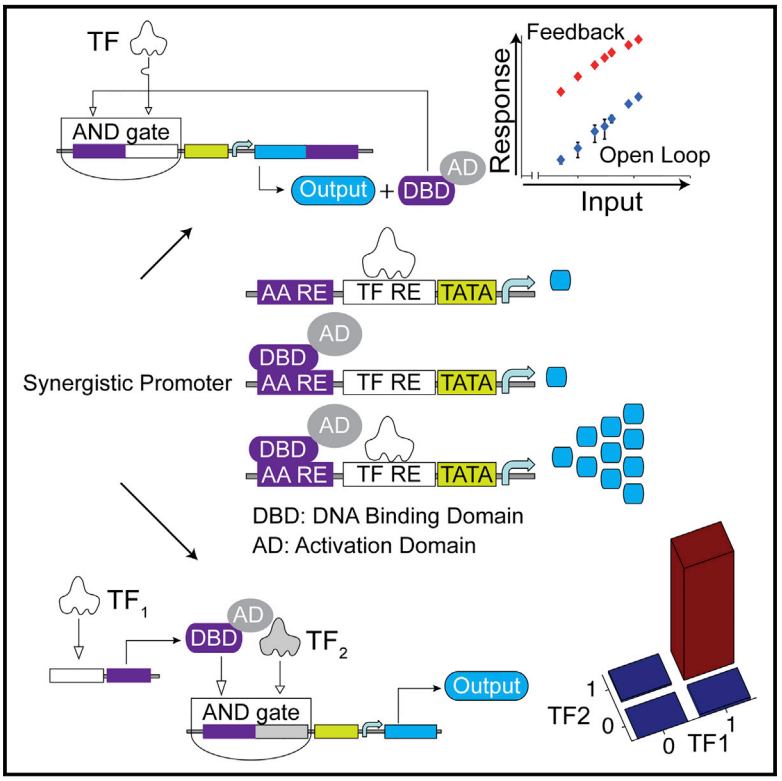

Authors

Bartolomeo Angelici, Erik Mailand, Benjamin Haefliger, Yaakov Benenson

Correspondence

kobi.benenson@bsse.ethz.ch

In Brief

Coupling endogenous transcription factor activities to synthetic gene circuits has been a longstanding challenge. Angelici et al. describe highly synergistic composite promoters that enable robust and selective amplification of mammalian transcriptional inputs using positive feedback as well as their arbitrary pairing in promoter-level AND gates. The resulting sensors can efficiently transduce their inputs' signal to downstream synthetic circuits via a variety of mechanisms, including RNAi, transactivation, and recombination.

Highlights

- A positive feedback loop with high synergy between trigger input and amplifier
- Rule-based design of robust amplified sensors of mammalian transcription factors
- AND gates between pairs of unrelated transcription factors
- Efficient transduction of transcriptional inputs into diverse downstream actuation

Angelici et al., 2016, Cell Reports *16*, 2525–2537
August 30, 2016
http://dx.doi.org/10.1016/j.celrep.2016.07.061

CellPress

Cell Reports
Resource

Synthetic Biology Platform for Sensing and Integrating Endogenous Transcriptional Inputs in Mammalian Cells

Bartolomeo Angelici,[1] Erik Mailand,[1] Benjamin Haefliger,[1] and Yaakov Benenson[1,2,*]
[1]Department of Biosystems Science and Engineering, Swiss Federal Institute of Technology (ETH Zurich), Mattenstrasse 26, 4058 Basel, Switzerland
[2]Lead Contact
*Correspondence: kobi.benenson@bsse.ethz.ch
http://dx.doi.org/10.1016/j.celrep.2016.07.061

SUMMARY

One of the goals of synthetic biology is to develop programmable artificial gene networks that can transduce multiple endogenous molecular cues to precisely control cell behavior. Realizing this vision requires interfacing natural molecular inputs with synthetic components that generate functional molecular outputs. Interfacing synthetic circuits with endogenous mammalian transcription factors has been particularly difficult. Here, we describe a systematic approach that enables integration and transduction of multiple mammalian transcription factor inputs by a synthetic network. The approach is facilitated by a proportional amplifier sensor based on synergistic positive autoregulation. The circuits efficiently transduce endogenous transcription factor levels into RNAi, transcriptional transactivation, and site-specific recombination. They also enable AND logic between pairs of arbitrary transcription factors. The results establish a framework for developing synthetic gene networks that interface with cellular processes through transcriptional regulators.

INTRODUCTION

Development of synthetic gene networks, or circuits, has tended to employ two complementary approaches. One approach focuses on the unique function of a gene circuit, e.g., biomanufacturing (Steen et al., 2010), complex dynamics (Elowitz and Leibler, 2000; Gardner et al., 2000; Stricker et al., 2008; Tigges et al., 2009), or information processing (Ausländer et al., 2012; Benenson, 2012; Deans et al., 2007; Friedland et al., 2009; Green et al., 2014; Park et al., 2003; Rinaudo et al., 2007; Tamsir et al., 2011). The cells in which these networks operate are viewed as relatively passive containers, or chassis. A complementary effort aims to alter or modify cellular processes by focusing on gene circuits that interface with the host cell, sensing endogenous inputs from the cell or environment and responding with specific biologically active outputs (Ausländer et al., 2014; Culler et al., 2010; Kobayashi et al., 2004; Nissim and Bar-Ziv, 2010; Slomovic and Collins, 2015; Xie et al., 2011). Such circuits are conceptually similar to regulatory or signaling pathways, with inputs typically conveying information about an internal or environmental cell state and thus driving a desired response.

Although known mechanisms are typically used to establish interactions between endogenous inputs and synthetic components, extensive engineering effort is often necessary to match the two. One example is a family of proportional microRNA (miRNA) sensors (Lapique and Benenson, 2014) that employ RNAi (Fire et al., 1998; McManus and Sharp, 2002). Mammalian transcription factors (TFs) comprise another family of well-studied (Janknecht et al., 1993; Kadonaga et al., 1987), information-rich cellular inputs (Hobert, 2008). Although researchers constructed used complex transcriptional regulatory building blocks and networks (Amit et al., 2011; Farzadfard et al., 2013; Khalil et al., 2012; Leisner et al., 2010; Li et al., 2015; Lienert et al., 2013; Maeder et al., 2013; Perez-Pinera et al., 2013), they have tended to employ non-native transcriptional inputs.

Here, we present a framework for systematic rational design of selective and robust sensing, integration, and transduction of endogenous TF activity in mammalian cells. We begin by describing a cell-based assay for characterization of TF sensor elements and their comparative analysis. We use five transcriptional activators, each tested with a panel of response elements (REs). Due to modest induction levels, we augmented the sensors with positive transcriptional feedback using an artificial amplifier activator and observed, counterintuitively, high response levels and low leakage. We dissect the behavior of composite promoters within this feedback loop and uncover high synergy between the feedback amplifier activator and the endogenous input of interest. As a result, the sensors do not function as binary switches (Xiong and Ferrell, 2003) that generate either very low or saturated output, depending on whether the input is below or above a certain threshold (all-or-none response). Instead, they are amplifiers whose output grows in proportion to the input. They operate well within the physiological activity range of the input. The initial dataset and computational analysis allow formulation of design principles that we illustrate using three additional TFs. We next show that high-synergy promoters can be employed for tunable two-input AND logic between unrelated TFs, requiring simultaneous activation by both factors to trigger a response. Furthermore, we demonstrate

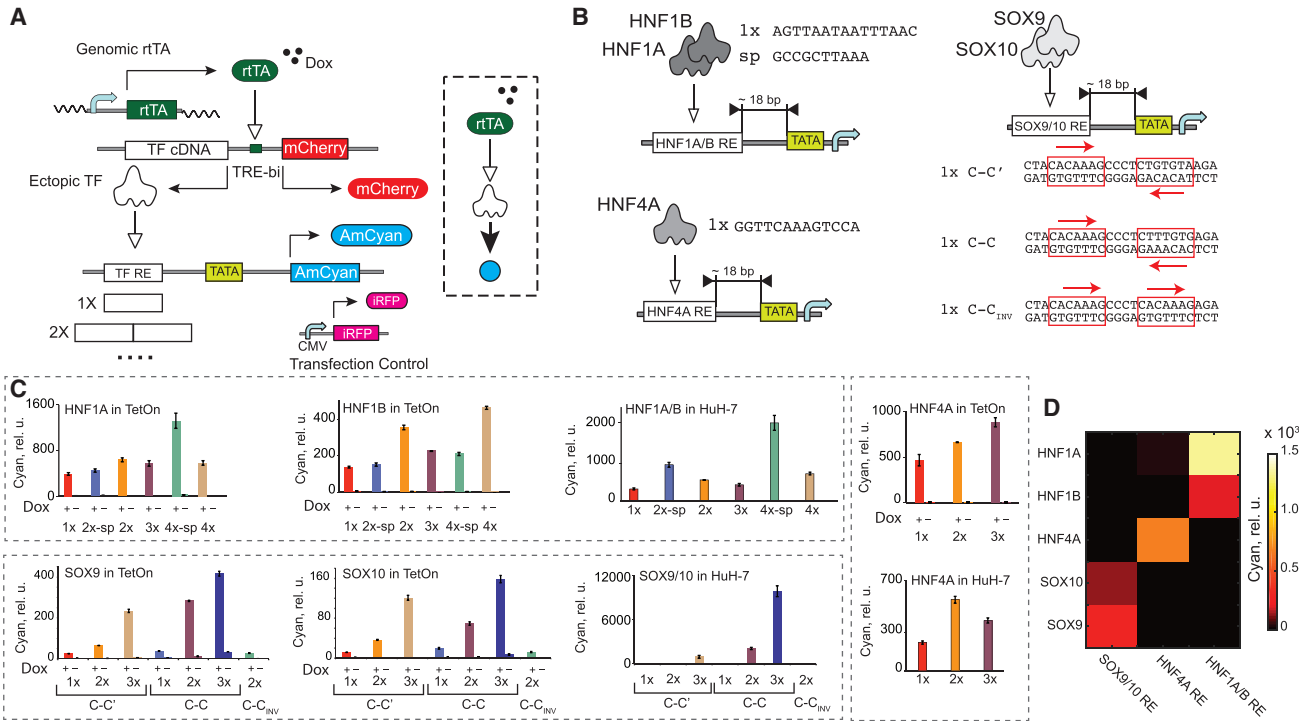

Figure 1. Characterization of Open-Loop Transcriptional Sensors

(A) Schematics of a sensor screening assay in HEK Tet-On cells. TATA indicates a core minimal promoter. DNA constructs and protein products are shown. Pointed arrow indicates transactivation.

(B) Schematics of the HNF1A/B, HNF4A, and SOX9/10 sensors. The sequences of 1× REs and a spacer (sp) are shown. Only top strands are shown for HNF1A/B and HNF4A.

(C) TF sensor population-averaged responses in HEK Tet-On cells in the presence and absence of Dox, as indicated, and in the HuH-7 cell line. Each bar represents mean ± SD of biological triplicates.

(D) Mutual crosstalk between the TFs (y axis) and sensors (x axis). The color code indicates averaged AmCyan intensity.

rtTA, reverse tetracycline-responsive transcriptional activator; CMV, cytomegalovirus promoter; TetOn, HEK293 Tet-On cells.

sensor utility in diverse scenarios such as miRNA induction, transactivation of downstream genes, and site-specific recombination. Our findings open the door to rational design of efficient and selective transcriptional sensors as part of downstream synthetic networks for sophisticated intervention into cell physiology.

RESULTS

Characterization of TF REs on a Neutral Background

We designed an assay (Figure 1A) to probe TF interactions with their REs and gauge their specificity and selectivity. In this assay, we transfect cells with two DNA cassettes. The first one comprises a bidirectional Tet RE (TRE) promoter controlling the cDNA of a TF input (Senkel et al., 2005) and an mCherry fluorescent reporter in a doxycycline (Dox)-dependent fashion, such that mCherry fluorescence can be used as a proxy for TF concentration. The second cassette (sensor) contains a TF binding site or sites cloned in front of a low-leakage minimal mammalian promoter (Hansen et al., 2014), driving an AmCyan fluorescent reporter. mCherry-AmCyan reporter pair allows indirect assessment of the input-output relationship between a TF and the regulated gene product (Kim and O'Shea, 2008; Rosenfeld et al., 2005). Initially, the inputs comprised liver-enriched hepatocyte nuclear factors (HNFs) HNF1A, HNF1B (Odom et al., 2004), and HNF4A (Dean et al., 2010) and developmental regulators SOX9 (Kadaja et al., 2014) and SOX10 (Zhou et al., 2014). We constructed panels of six REs for HNF1A/B (Senkel et al., 2005; Tronche et al., 1997), three REs for HNF4A (Fang et al., 2012), and seven REs for SOX9/10 (Peirano and Wegner, 2000), with elements differing in the number of binding site repeats, their sequence, and their spacing (Figure 1B). We use HEK293 Tet-On (HEK Tet-On) cells that do not express these factors endogenously (Kikuchi et al., 2007; Küspert et al., 2012; Lucas et al., 2005; Wissmüller et al., 2006) but enable their Dox-dependent ectopic induction.

Population-averaged "off" responses (Figure 1C) with zero Dox confirm the lack of endogenous expression of all five factors in HEK Tet-On cells. The "on" values (saturated Dox) obtained with different REs uncover diverse behaviors of the cognate TFs. HNFs exhibit sublinear (Zhang and Andersen, 2007) dependency, whereby doubling the number of binding sites results in a less than double output increase. HNF1A is stronger than HNF1B, consistent with earlier observations (Kitanaka et al.,

2007). However, the SOX factors show superlinear activation, with output-level fold change surpassing the binding site number fold change. This suggests synergy between TFs bound to individual sites (Perez-Pinera et al., 2013; Smith et al., 2013). The data also support previous in vitro observations in favor of two high-affinity sites, C-C (Peirano and Wegner, 2000), and confirm the importance of cooperative SOX9 and SOX10 dimerization, judging from the low response of monomer-binding C-inverted C ($C\text{-}C_{inv}$) RE. To test sensors' response to physiological TF level, we transfected them into a HuH-7 liver cancer cell line that expresses HNF1A/B, HNF4A, and SOX9/10 (Figure 1C). The activity of various REs in this context recapitulates to some extent the behavior in HEK Tet-On cells, with the best responders in HEK cells remaining the best responders in HuH-7 cells (apart from a change in ranking with HNF4A). However, quantitatively, the responses do not correlate well between the two cell types, likely due to additional modulating interactions between TF inputs and cell background in HuH-7. In particular, the SOX9/10 3× C-C site works better in HuH-7 cells compared to 3× C-C′, while its relative advantage in HEK Tet-On cells is only 2-fold. Members of the SOX-E group (SOX8, SOX9, and SOX10) share sequence homology in the DNA binding domain (Wegner, 2010), and this difference in response may be ascribed to sensor interaction with other members of the group in HuH-7 cells. Finally, we evaluated mutual cross-activation in this library of transcription factors and response elements in HEK Tet-On cells. The resulting matrix (Figure 1D) is consistent with the expectation, showing only the expected cross-reactivity between TFs with homologous DNA binding domains.

Flow cytometry data in transient transfection can be binned and averaged by the input (mCherry) intensity to build the transfer curve that shows the relationship between the TF level inferred from the mCherry reporter and the output AmCyan (Bleris et al., 2011). The curves measured with the same TFs have similar shape after normalization (Figure S1A). A simple model (Supplemental Experimental Procedures) predicts that the curve can be quadratic at low and linear at high TF/mCherry levels (Equation 1):

$$[AmCyan] = \frac{[mCherry]^2}{b_1 + b_2[mCherry]} + b_3. \quad (1)$$

However, only HNF4A and HNF1A fit this prediction. HNF1B, SOX9, and SOX10 exhibit increasing deviations that are well described by a saturating rational function (Equation 2):

$$[AmCyan] = \frac{[mCherry]}{a_1 + a_2[mCherry]}. \quad (2)$$

Accordingly, the observed behavior is a superposition of the responses described by Equations 1 and 2 (Figure S1B). In a cotransfection, dependency (Equation 2) is characteristic of an incoherent feedforward regulation (Bleris et al., 2011), and we speculate that TFs with the highest deviation might also act as negative regulators of their output by either repression or steric hindrance of the compact promoter region (Cruz-Solis et al., 2009). The transfer curve shape provides information on reporter response to different TF levels, and its deviation from a simple prediction can justify further mechanistic studies.

Signal Amplification using Positive Feedback

The sensors we characterized earlier are simple open-loop systems in which the signal propagates sequentially. They generate low absolute output levels that might not suffice to transduce a TF signal into robust downstream actuation. A positive feedback, whereby the output positively regulates its own expression, can amplify the output relative to the open-loop scenario (Acar et al., 2005; Ajo-Franklin et al., 2007; Alon, 2007; Becskei et al., 2001; Enciso and Sontag, 2005; Tan et al., 2009), with the caveat that weak output leakage in the absence of an input can self-amplify and lead to output saturation. Because our output is a fluorescent protein, we had to couple its expression to a transcriptional transactivator we call an amplifier activator to establish the feedback. We attempted to reduce autoinduction using low-leakage REs in combination with a low-leakage minimal promoter and low-leakage, shallow dose-response DNA regulatory elements for the amplifier activator. The open-loop sensors satisfied the first requirement; for the amplifier activator, we chose the pristinamycin I-dependent transactivator (PIT)2/pristinamycin I-repressible promoter (PIR) system (Fussenegger et al., 2000) with reduced sensitivity to small amounts of activator (Prochazka et al., 2014). In summary, we established the positive feedback by cloning a 2A linker and PIT2 transactivator downstream of the AmCyan reporter and a PIT2 DNA binding site (PIR) upstream of the TF RE (Figure 2A).

We first characterized feedback-amplified sensors in the HEK Tet-On assay (Figure 2B). The absence of a TF cassette (TF^{NEG}) was required to faithfully represent the off state because of TRE promoter leakage in the absence of Dox (Dox^{-}). The induction ratios against the TF^{NEG} background range from 10 to 700 (Figure S2C; Table S1). Sensor performance depends on the TF input and the RE sequence, with the strongest leakage in the off state and the lowest on-to-off ratio observed with 1× REs, in which the PIR is closest to the TATA box. This ratio increases as the PIR site is pushed farther away, reaching about 350-fold on average in feedback-amplified sensors with ≥3× REs. Likewise, the amplified sensors respond strongly to endogenous TF inputs in HuH-7 cells (Figure 2B). The amplification relative to the open-loop sensors and the absolute induced levels vary between TFs and cell lines. As an illustration, the 3× C-C SOX10 amplified sensor shows comparable response in Huh-7 and HEK Tet-On cells, while its open-loop version responds more strongly in HuH-7 cells relative to HEK Tet-On cells. In HuH-7 cells, all HNF1A/B amplified sensors behave similarly, but this is not so in HEK Tet-On cells.

We next evaluated the mutual orthogonality of the amplified sensors. The resulting matrix (Figure 2C) shows crosstalk between the HNF1A/B TFs and the amplified HNF4A sensor that was not observed with the open-loop sensors. The DNA binding domains of the two TFs are highly divergent, and members of the HNF1 family are unable to bind to HNF4A RE. However, it has been shown that some tissues exhibit HNF1-dependent HNF4A expression (Boj et al., 2001; Thomas et al., 2001) and that ectopic expression of HNF1A/B in an HNF4A-negative cell line (3T3) induces an HNF4A isoform from a distal promoter (Briançon et al., 2004).

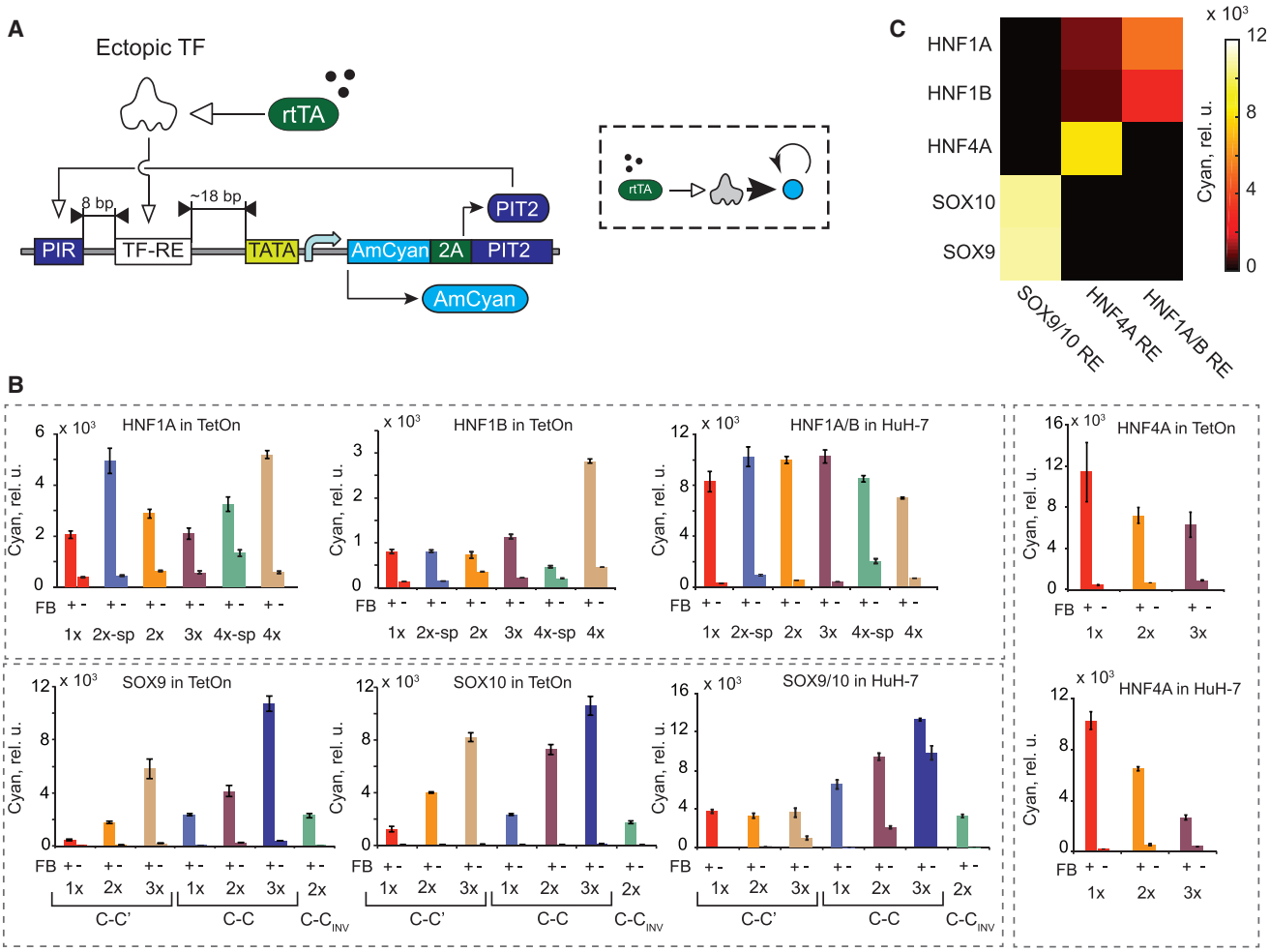

Figure 2. Initial Characterization of TF Sensors with Positive Feedback

(A) Schematics of a feedback-amplified TF sensor.

(B) Induction levels measured in HEK Tet-On cells and in HuH-7 cells compared to their open-loop counterparts (values reproduced from Figure 1). TF and cell line names are indicated. Open-loop and amplified sensor outputs are directly comparable, but the amplified output signal is underestimated by a factor of five due to the 2A sequence (Figure S3B). FB, feedback; TetOn, HEK293 Tet-On cells. Each bar represents mean ± SD of biological triplicates.

(C) Crosstalk between the feedback-amplified sensors and different input TFs.

Mechanistic Dissection of Feedback Amplifiers

The amplified and open-loop sensor outputs correlate in HEK Tet-On cells (Figure 2). This is contrary to an intuitive expectation that the induced levels would be identical when the same sensor is triggered by different TF inputs due to the autocatalytic positive feedback. In an attempt to explain these observations, we mutated PIT2 to eliminate the feedback loop (Figures S3A and S3B) and measured the response of the composite promoters driving the output to different combinations of the ectopic TF and the amplifier activator (Figures 3A and 3B; Figure S3C). In most cases, the ectopic TF input or the amplifier activator alone triggers low response. A stronger synergistic activation, up to 50-fold higher than expected from adding individual contributions, was measured when both TF and amplifier activator were present (Figure 3C). The 3-fold synergy on a composite promoter comprising activating transcription factor and upstream activating sequence binding sites in HeLa cell extracts (Lin et al., 1990) and synergies on natural promoters (Smith et al., 2013) were previously reported, but the magnitude of the effects here surpasses earlier observations, leading to a high-performance AND gate between the amplifier activator and the TF input.

We further dissected this phenomenon by varying different components of the composite promoter and/or the activator species. We replaced the transactivating domain RelA of PIT2 (otherwise denoted PIT-RelA) with VP16 (Figure S3D), the PIT DNA binding domain with the erythromycin (ET) binding domain (Weber et al., 2002) (Figures 3D and 3E), and the minimal promoter sequence with a minimal cytomegalovirus promoter (CMV_{MIN}) (Figure 3F). Replacing the transactivating domain improved the synergy due to a reduced efficiency of PIT-VP16 alone at longer distances from the TATA box. Synergy was not

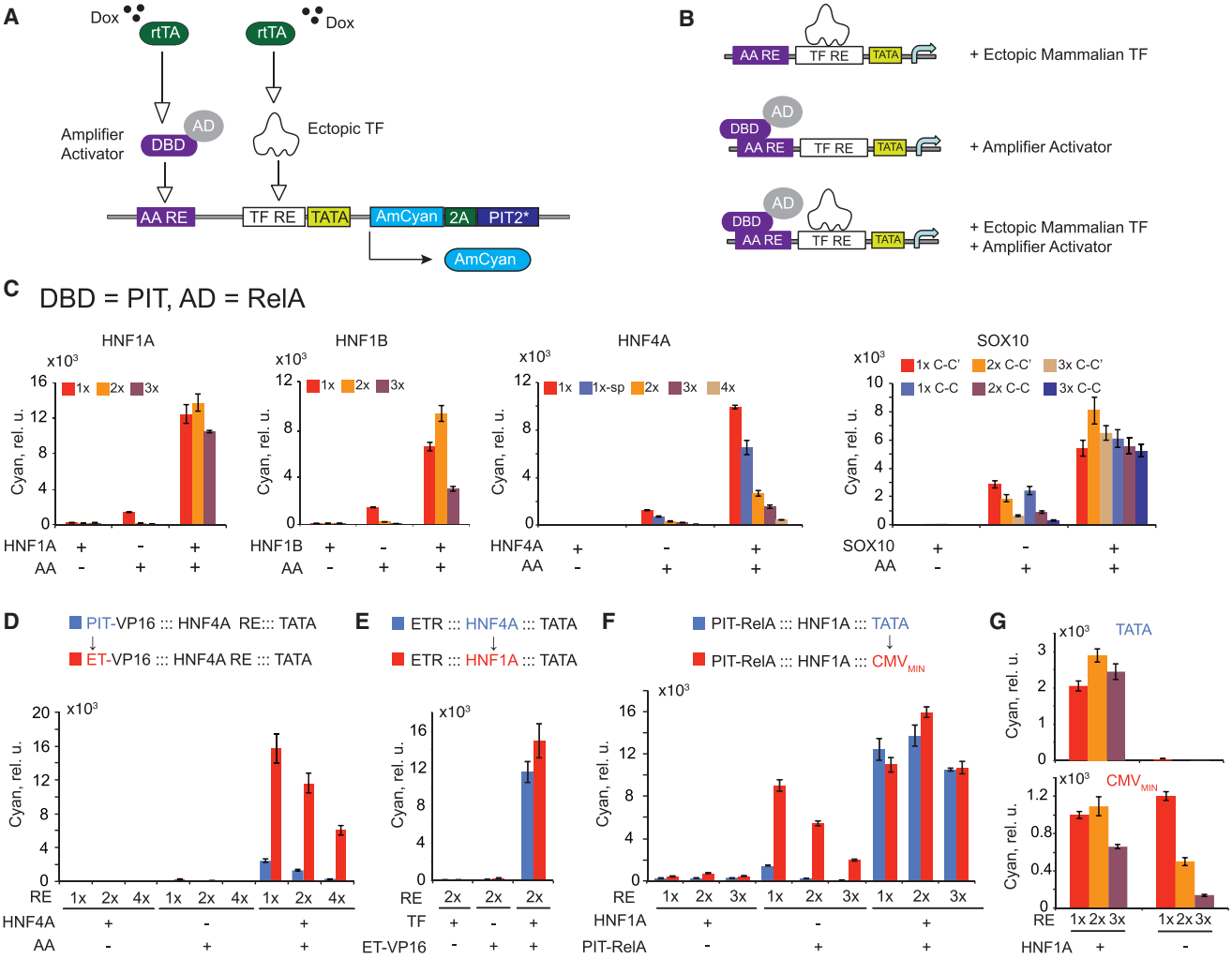

Figure 3. Characterization of the Composite Promoters

(A) Experimental layout. Both the ectopic mammalian TF and the amplifier activator are induced with Dox. Different combinations of transcriptional inputs are achieved by withholding either the TF- or the amplifier activator-expressing cassette.

(B) Schematics of different transcriptionally active complexes. DBD, DNA binding domain; AD, activation domain.

(C) Expression levels reached with either or both transcriptional inputs provided to the promoter, as indicated. Different REs are compared.

(D) Effect on synergy of swapping the DBD of the amplifier activator from PIT to ET for three REs of HNF4A.

(E) Effect on synergy of replacing the TF input and its RE without changing the amplifier activator ET-VP16.

(F) Effect on synergy of swapping the minimal promoter from the minimal TATA box to CMV_{MIN}.

(G) Comparison between feedback-amplified sensors harboring a minimal TATA box (top) and those harboring CMV_{MIN} (bottom) with and without the TF input. 1×, 2×, and 3× HNF1A/B REs are compared.

In all panels, each bar represents mean ± SD of biological triplicates.

affected when we swapped the amplifier activator and the corresponding DNA binding domain, pointing to the general nature of the synergistic activation and the possibility to use multiple amplifier activators in parallel. However, replacing the minimal TATA box with CMV_{MIN} reduced synergy dramatically due to increase in the induction by the amplifier activator alone. CMV_{MIN} also had a large detrimental effect on the amplified sensors, which are almost fully induced even in the absence of a TF input (Figure 3G). With a minimal TATA box, the synergy was confirmed in two additional cell lines, HeLa and HCT-116 (Figure S3E).

The induction by PIT2 alone decreases with distance between the PIR and the TATA box. The magnitude of PIT2-only induction also depends on the downstream TF REs (Figure 4A). Promoters with HNF REs behave similarly, while promoters with SOX9/10 REs generate somewhat higher expression. We did not find obvious sequence features that could explain this difference. With CMV_{MIN}, the PIT2-only induction is higher (Figure 4A, inset). One explanation is the binding of cryptic endogenous TFs to either the REs or the minimal promoters. Spurious binding can be estimated from the leakage of the feedback-amplified sensors in the absence of their cognate TFs. However, there is no

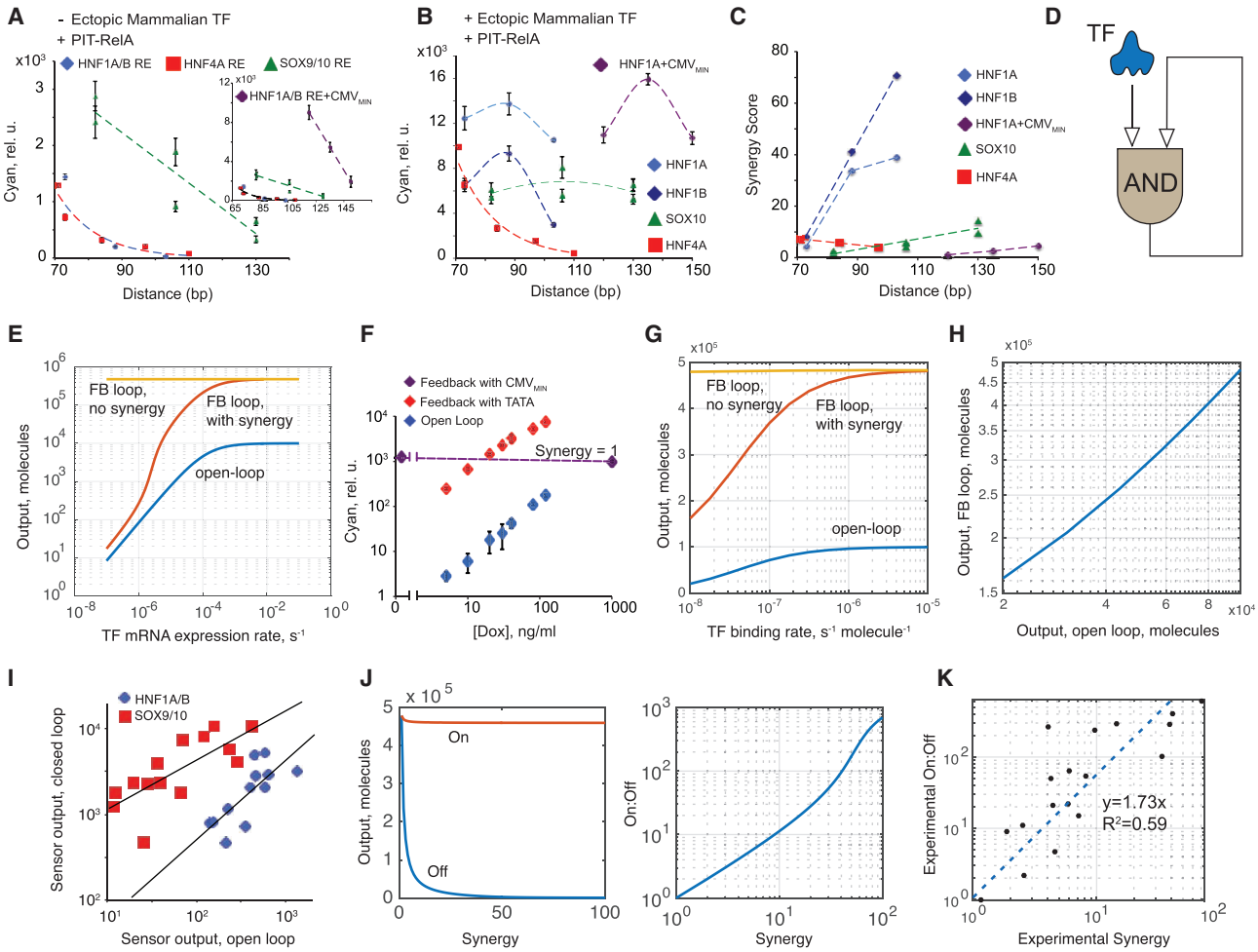

Figure 4. Analysis of Synergy Data

Synergy is calculated as a ratio of the expression in the presence of both TF and amplifier activator, divided by the sum of expression with TF only and amplifier activator only. To increase accuracy, TF-only data from Figure 1 is used for calculations (Supplemental Experimental Procedures).

(A) Transactivating efficiency of PIT-RelA amplifier activator as a function of PIR distance from the TATA box. The intervening RE for the endogenous TF input coupled to the low-leakage promoter (color coded) and the sequence of a minimal promoter (minimal TATA box versus CMV_{MIN}, inset) are compared.

(B) Fully induced expression levels from a composite promoter achieved by providing the ectopic TF input and PIT-RelA, as a function of PIR distance from the TATA box.

(C) Synergy scores for different composite promoters with PIT-RelA as amplifier activator, as a function of PIR distance from the TATA box.

(D) Schematics of the synergistic positive-feedback amplifier.

(E and F) Simulated (E) and experimental (F) responses of open- and feedback-amplified sensors to varying TF input. Comparison to an amplified loop without synergy is shown.

(G) Simulated open-loop and amplified response dependency on the binding affinity of the TF input.

(H) Simulated relationship between open- and amplified-loop responses.

(I) Experimental correlation between open- and closed-loop responses for HNF1A/B and SOX9/10 constructs in HEK Tet-On cells.

(J) Simulated off and on responses of feedback-amplified loops as a function of synergy (left) and on-to-off ratio as a function of synergy (right).

(K) Experimental on-to-off ratio of feedback-amplified sensors as a function of synergy (black dots). The straight line is a linear fit forced through zero.

In (A), (B), and (F), error bars represent SD of biological triplicates.

correlation between this leakage and PIT2-only induction (Figure S4A, top) in sensors furnished with the minimal TATA box, suggesting that the intervening sequence affects PIT2 transactivation potential. However, clear correlation exists between leakage from amplified sensors and PIT2 induction from composite promoters furnished with CMV_{MIN} (Figure S4A, bottom), strengthening the hypothesis that there is spurious binding to CMV_{MIN} acting as a hidden input to the otherwise synergistic regulatory sequences. This is supported by independent evidence of CMV_{MIN} leakiness (Prochazka et al., 2014).

Synergized output expression triggered by the combined action of PIT2 and TF input is roughly constant for HNF1A, HNF1B, and SOX10. For HNF4A, however, synergized expression declines with distance, similar to PIT2-only induction

(Figure 4B). Replacing RelA with the VP16 transactivation domain preserves the trends but not the absolute values. Activation strength by PIT-VP16 alone is reduced about 10-fold relative to PIT-RelA at short distances (Figure S4B). However, in a synergistic induction, most of this loss is recovered, reaching between 25% and 77% of the PIT-RelA values (Figure S4C). Therefore, the absolute synergy levels are in general higher when PIT-VP16 is used (Figure S4D). The exact dependency of synergy on distance varies between TF inputs (Figure 4C), but all constructs share substantial synergy.

High synergy in feedback-amplified sensors creates a regulatory motif, in which positive feedback is integrated in an AND-like gate with the external TF input (Figure 4D). We built a mechanistic model of this motif (Figure S4E; Supplemental Experimental Procedures). The simulation shows that the open-loop and the synergistic feedback sensors respond gradually to increasing input, while a sensor without synergy generates a fully induced response to non-zero inputs (Figure 4E; Figure S4F). This agrees with the responses of open-loop and amplified HNF1A sensors in HEK Tet-On cells to Dox-modulated HNF1A input. Both increase proportionally to the input while maintaining a constant amplification ratio (Figure 4F). However, an amplified sensor without synergy generates constant output (Figure 4F). The simulation also predicts strong correlation between the output in the open and that in the amplified synergistic loops (Figures 4G and 4H), in agreement with observations (Figure 4I). The output of the amplified sensor remains proportional to the output of the open-loop sensor, with the important practical implication that the amplified sensor is no longer a bistable on-off switch (as is the case in feedback loops without synergy). Instead, it is a proportional signal amplifier, multiplying input signal intensity by a constant value over a range of inputs. Lastly, the model predicts a proportional, if non-linear, relationship between the composite promoter synergy and the dynamic range of the amplified sensor, with the off state being most sensitive to synergy (Figure 4J). Experimental data (Figure 4K) agree qualitatively with this prediction.

Forward Sensor Design

The simulations and the experimental data reported earlier enable rational design and optimization of low-leakage feedback amplifiers. The empirical linear fit of the dataset in Figure 4K is $log_{10}(on:off) = 1.73 log_{10}(synergy)$ or $on:off = 53.7^{log_{10}(synergy)}$. This means that a synergy score of five or more will result in a satisfactory on-to-off ratio of the amplified sensor (~16), while scores > 10 will enable excellent induction of ~50. Thus, the task of designing an amplified sensor is reduced to finding the composite promoter of appropriate synergy. The data in Figures 3 and 4 suggest that although specific trends vary among TFs, it is possible to achieve sufficient synergy either by modulating the length of the RE and the distance between the TATA box and the amplifier activator biding site or by altering the transactivating domain of the amplifier activator. For new sensors, this dependency of synergy on distance should be mapped using two to three composite promoters that differ in the number of TF REs; the latter can be obtained from experimental probability weight matrixes (Jolma et al., 2013) and available literature. These promoters are evaluated under three conditions, AA^-/TF^+, AA^+/TF^-, and AA^+/TF^+, resulting in nine distinct measurements. A promoter with the highest synergy can then be used in an amplified sensor. We tested this approach with three additional transcription activators: TCF/LEF family, downstream effectors of the Wnt pathway (Buckley et al., 2015; Veeman et al., 2003), the hypoxia inducible factor HIF1A (Schödel et al., 2011), and calcium-sensitive NFATC1 (Fiering et al., 1990). TCF/LEF and HIF1 are expressed in HEK Tet-On cells but are only activated in response to their respective pathways' ligands (LiCl activating the Wnt pathways and $CoCl_2$ mimicking the hypoxic state), while NFATC1 is not expressed in HEK Tet-On. Accordingly, we relied on pathway activation to induce TCF/LEF and HIF1 and used a combination of cDNA of the calcium-sensitive NFATC1 mutant (CA-NFATC1) and calcium influx (stimulated by ionomycin) for NFATC1 induction. The composite promoter's behavior shows the requisite synergy levels (Figure 5A–5D), and all amplified sensors behave satisfactorily, better than expected from the preceding empirical dependency (Figure 5E). Promoter mapping is useful for uncovering trends, yet as a rule, sensors for which the RE pushes the amplifier activator about 110 bp away from the TATA box show a combination of high induction in the on state and a high on-to-off ratio (Figures 2, 5, and S2C); if time is of the essence, then only one structure with 3× or 4× RE repeats and a corresponding separation of 100–130 bp can be tested.

The preceding workflow requires that the TF be inactive in the ground off state. Although cell lines such as HEK Tet-On naturally lack either expression or activity of certain TFs, establishing a clean ground off state in the most general case might require a homozygous deletion of the gene encoding the TF of interest. In addition, it requires the ability to turn on the TF in a controlled fashion by ectopic expression using cDNA, a cofactor as an "on" switch, or both. This ability can be compromised when a crucial cofactor is unknown.

Synergistic Promoter Enables Transcriptional Logic

To further decipher the AND-like behavior of the synergistic composite promoters, we mapped their response to gradual changes in the transcriptional inputs. The ectopic TFs were tuned with Dox via the TRE promoter, while the amplifying activators PIT-RelA and ET-VP16 were expressed from constitutive promoters and modulated with the antibiotics pristinamycin (PI) and erythromycin (ET), respectively. As expected, the responses fit Dox AND NOT (antibiotic) logic between the small molecule inputs, consistent with the underlying ectopic TF AND amplifier activator promoter logic (Figure 6A). The AND-gate promoters can be used to build AND gates between pairs of unrelated mammalian TFs, with one controlling the amplifier activator and the other controlling its cognate RE directly (Figure 6B). We tested this circuitry in HEK Tet-On cells by either adding or withholding plasmids expressing the TFs of interest. The gate HNF1A AND SOX10, using PIT-RelA as the amplifier activator, generates the worst-case on-to-off ratio of ~16 (Figure 6C). The HNF4A AND SOX10 gate with PIT-RelA gives the worst-case on-to-off ratio of ~5. However, replacing PIT-RelA with PIT-VP16 increases the on-to-off ratio to ~40-fold, consistent with the higher synergy expected from PIT-VP16 (Figure 6D). The AND-gate behavior observed in HEK Tet-On cells can also be exploited for identifying simultaneous expression of

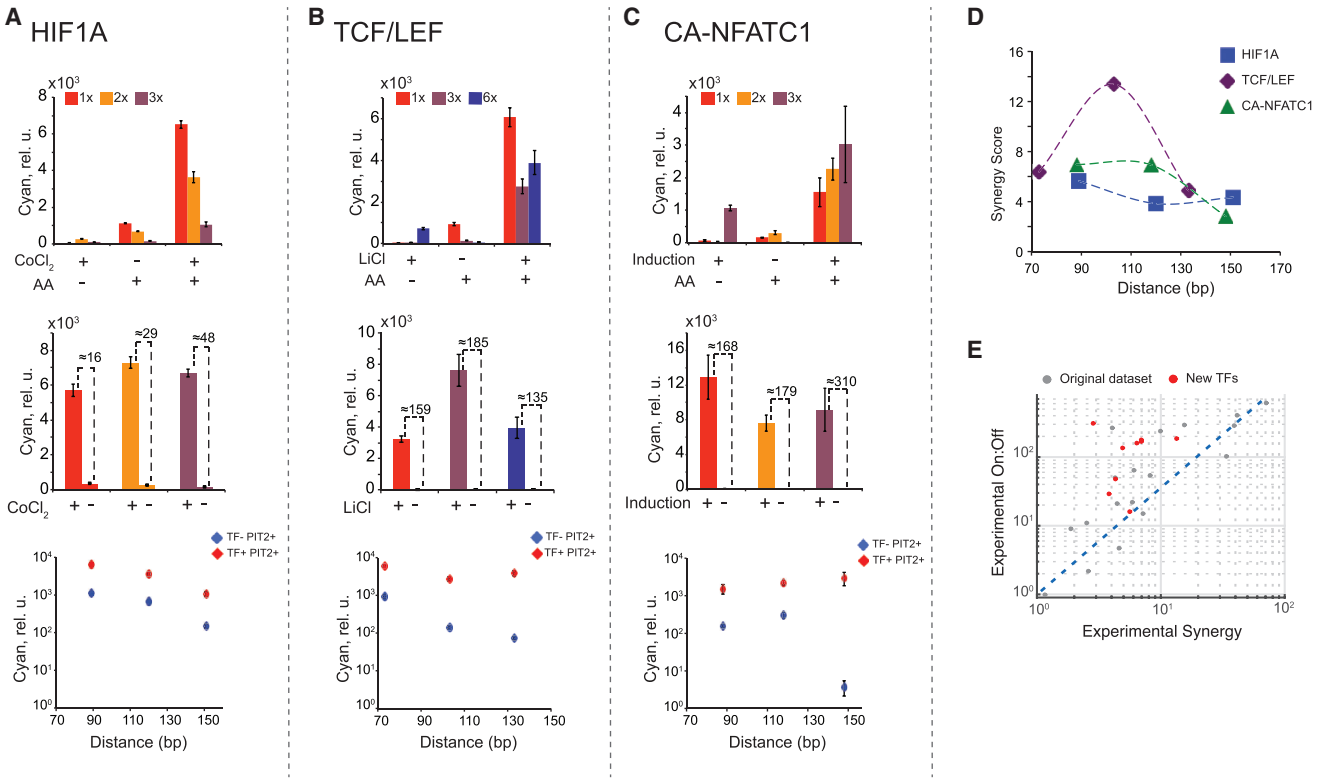

Figure 5. Forward Sensor Engineering

(A–C) For each TF, we show the response of the composite promoter in open-loop configuration (top) and the response of the corresponding feedback loops (middle) and then compare the distance dependency of PIT-RelA transactivation with the synergized expression (bottom). The cofactors used for induction are indicated. For NFATC1, induction means expression of the TF cDNA combined with ionomycin.

(D) Synergy for the composite promoters tested in this panel as a function of PIR distance from the TATA box.

(E) On-to-off ratio as a function of synergy for this dataset (red), overlaid on Figure 4K data (gray).

In (A)–(D), error bars represent SD of biological triplicates.

endogenous TFs. The HNF1A/B AND SOX9/10 gate was applied to a panel of cell lines including HuH-7, HCT-116, HEK293, and HeLa. In this panel, only HuH-7 cells express both factors, and HuH-7 is the only cell line that strongly activates reporter expression (Figure 6E).

Amplified Sensors as Transducers of Biological Activity

Having established selective and strong output activation by endogenous TFs, we attempted to transduce it to other types of biological activity. First, we tested the ability of the open-loop and the amplified sensors to induce a synthetic miRNA miR-FF4 and knock down gene expression in response to endogenous HNF1A/B in Huh-7 cells (Figure S5A). Knockdown efficiency elicited by the open-loop sensor was only ~3.5-fold (Figure S5B), improving somewhat with an amplified sensor (Figure S5C). The improvement was smaller than the concomitant increase in the AmCyan and miR-FF4 levels, consistent with earlier observations on RNAi knockdown kinetics in the case of simultaneous miRNA and target expression from transfected constructs (Lapique and Benenson, 2014). Briefly, the miRNA target protein commences expression immediately and builds up high background levels during the time it takes to accumulate sufficient miRNA to elicit efficient knockdown. With feedback amplification, the delay between transfection and miRNA accumulation is expected to be even longer. We employed the internal desynchronization method using a Cre recombinase inversion of the output described earlier (Lapique and Benenson, 2014) and, as expected, observed a robust knockdown of about 20-fold of downstream target (Figures 7A and 7B).

The amplifier activator can be used to transactivate additional genes via suitable promoter; combined with miRNA expression, this enables simultaneous and anticorrelated control of two or more genes conditioned upon a single transcriptional trigger (Figure S6). To illustrate this, we constructed a PIR_{TIGHT}-controlled (Hansen et al., 2014) mCitrine cassette and combined it with the amplified HNF1A/B sensor and miR-FF4 targeted mCherry gene. The circuit was tested using HuH-7 as a HNF1A/B-positive cell and HEK293 and HeLa as HNF1A/B-negative cells. We find that all outputs behave as expected, with Cyan and Citrine highly expressed in HuH-7 cells and mCherry high in HEK293 and HeLa cells (Figure 7C). The fold change is between two and three orders of magnitude, with the best case as 320-fold AmCyan induction in HuH-7 versus HEK293 and the worst case as a 20-fold difference in Citrine between HuH-7 and HEK293 cells.

Another common application of sensor systems is irreversible cell marking using site-specific recombination. We substituted

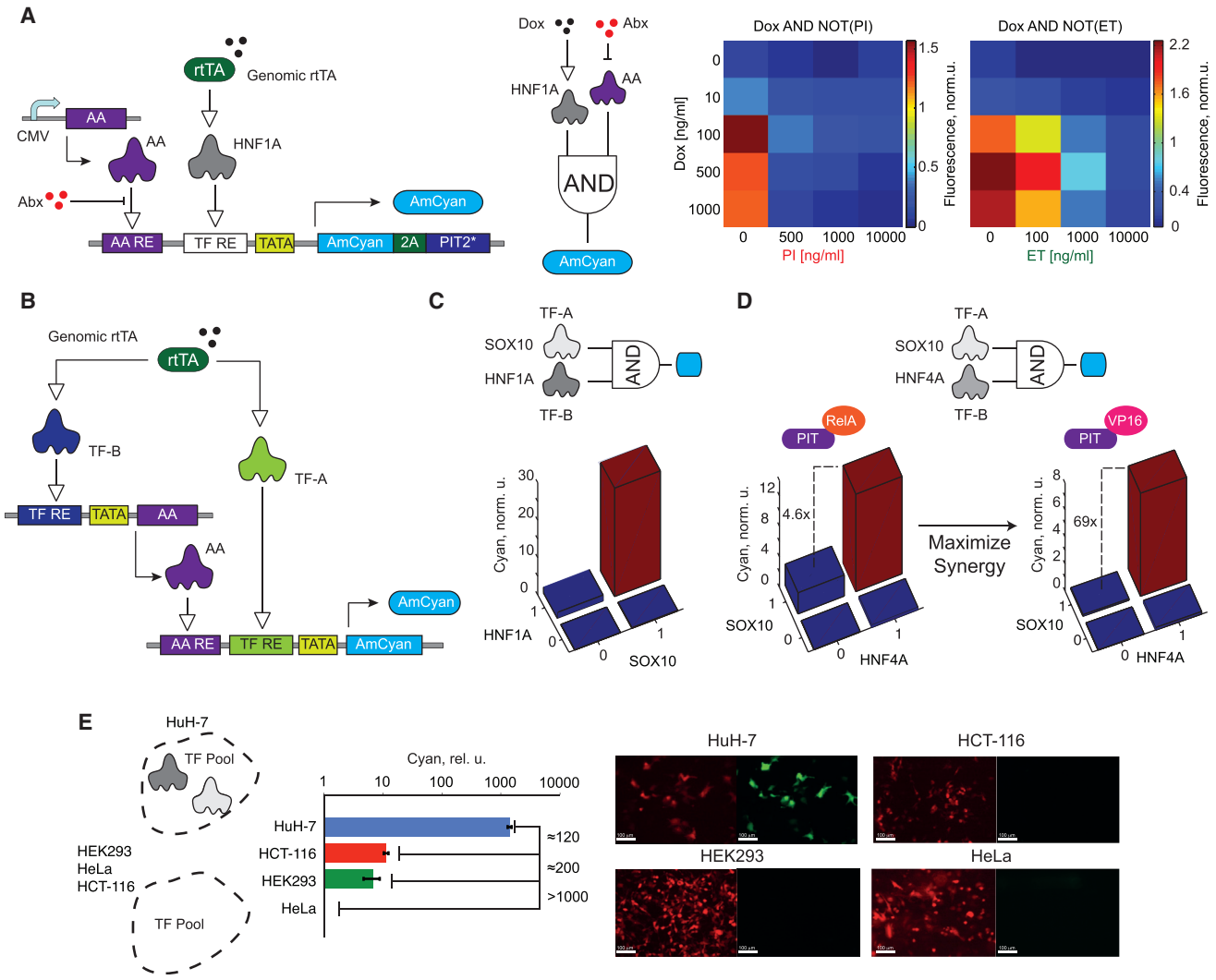

Figure 6. AND Logic on the Composite Promoter

(A) Experimental setup for independent input modulation and the logic circuit abstraction of this setup (left). Promoter response as a function of varying levels of the TF and the amplifier activator inputs (right). Abx, antibiotic; PI, pristinamycin; ET, erythromycin.

(B) Schematics of an AND gate between two ectopic transcriptional inputs.

(C) AND gate between SOX10 and HNF1A.

(D) AND gate between HNF4A and SOX10. Left, the gate that used PIT-RelA. Right, the same gate employing PIT-VP16.

(E) AND gate between HNF1A/B and SOX9/10 discriminates between cell lines using endogenous levels of TF inputs. The bar chart shows AmCyan output levels in different cell lines (each bar represents mean ± SD of biological triplicates), and the micrographs show the expression of transfection marker mCherry (red) and the AmCyan output (green). Scale bars, 100 μm.

AmCyan with a Cre recombinase (Figure 7D) to evaluate this scenario, testing amplified sensors for both HNF1A and SOX10 (Figure 7E). We observe highly specific TF-dependent recombination resulting in a 10- to 25-fold Citrine induction in the HEK Tet-On assay and up to 100-fold selectivity in Huh-7, with endogenous transcriptional inputs with virtually zero leakage in the TF-negative cells (Figure 7F).

DISCUSSION

Our study establishes a methodology for using endogenous TFs as input signals to artificial gene circuits in mammalian cells. The assay based on ectopic coexpression of the transcriptional input of interest, together with a fluorescent protein, provides an information-rich platform that can be used both for bulk comparison of different REs and for their in-depth characterization using binned response curves. In particular, the latter can point to deviations of measured behavior from simple mechanistic models and justify further studies. The assay can likewise be used to validate observations made in natural contexts or in vitro and to deconvolve complex behaviors by isolating the effects originating from putative interaction partners. Use of amplified sensors on a neutral background is a sensitive detector of direct and indirect crosstalk that is otherwise missed in open-loop sensors. The

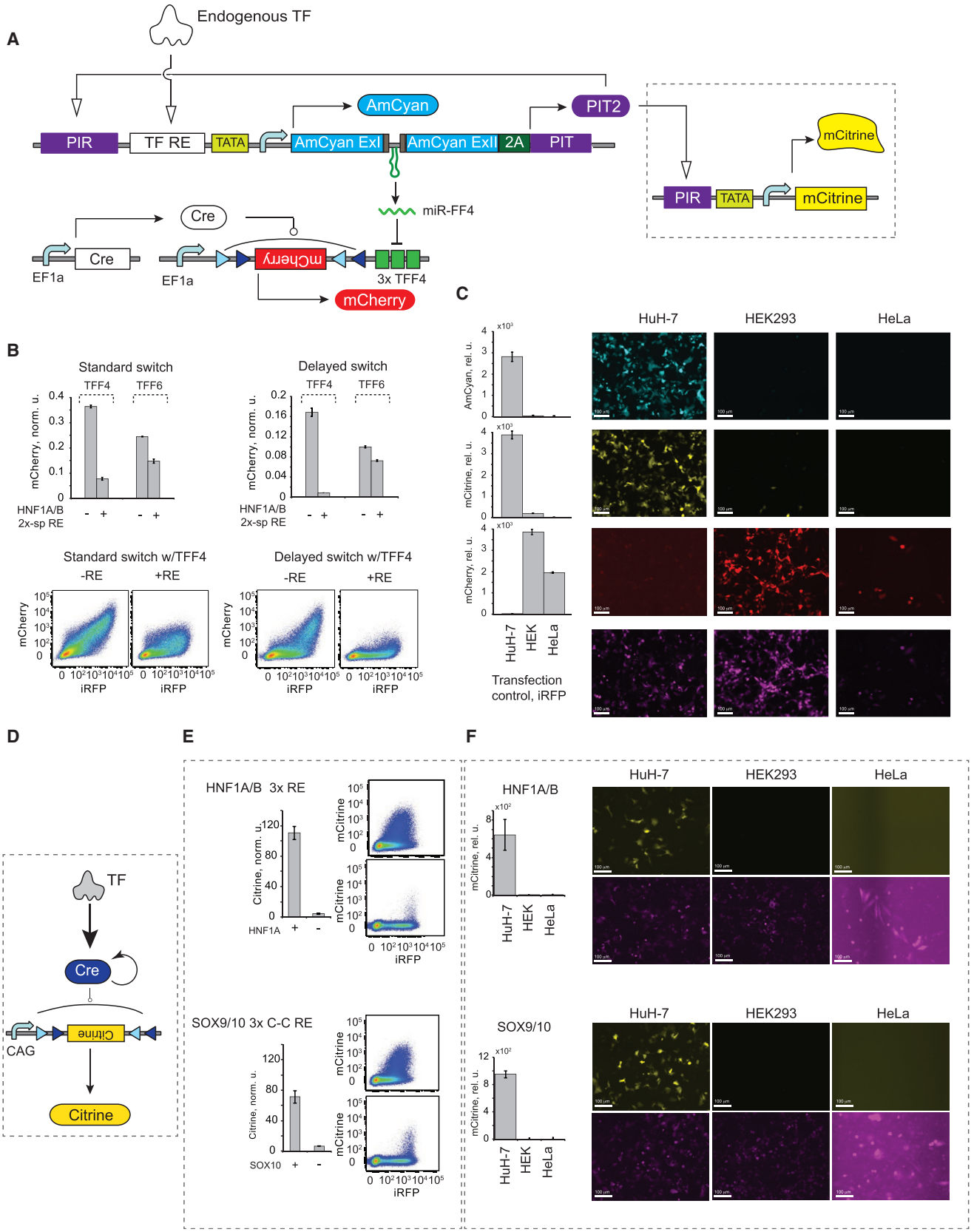

(legend on next page)

extension of this assay can encompass application-specific cell types (such as induced pluripotent stem cells (iPSCs)), in which the TF of interest is deleted genetically, preserving the rest of the cell background relevant to this application. However, cofactors can be studied quantitatively in a cell line such as HEK Tet-On by inducible ectopic expression of the cofactors, together with the studied TF. In summary, our assay can complement other approaches (Dean et al., 2010; Olson et al., 2014; Patwardhan et al., 2012; Peirano and Wegner, 2000; Sharon et al., 2012) by providing complete control over the TF input, its cofactors, and the structure of the RE.

We further establish a robust, programmable, modular tool for transcriptional signal amplification, with the help of the AND-gate positive-feedback sensor. Although synergies between transcriptional inputs on promoters have been observed previously, we reach very high levels that justify the interpretation of the behavior as a logic AND gate. Combining high synergy with positive feedback generates a proportional signal amplifier, unlike previously described binary switches. We show that the induction ratio of the amplified sensor is proportional to the synergy levels on the promoter. We suggest a workflow to tune the ratio based on systematic dissection of different parameters and apply it successfully to three additional TFs. The AND-gate promoter also leads to two-input AND gates between pairs of unrelated transcriptional inputs with high on-to-off ratios. We were able to improve the performance of these gates using our design rules.

Most constructs and functionalities are confirmed in the HuH-7 cell line with physiological input levels. The amplified sensors were able to trigger efficient multipronged biological actuation in the form of RNAi, transactivation, and site-specific recombination. These sensing and transduction capabilities fill the missing link between endogenous transcriptional activities and previously established strategies to implement transcriptional logic (Hansen et al., 2014; Khalil et al., 2012; Leisner et al., 2010; Ran et al., 2012), and they will facilitate construction of logic circuits of increasing complexity. Logic gates between arbitrary TFs could enable specific cell targeting based on complex transcriptional profiles, further contributing to the ongoing effort toward improving tissue- and lineage-specific transgene expression in mammalian cells, with applications in basic research (Halpern et al., 2008) and gene therapy (Busskamp et al., 2010). Given the central role of TFs in cell fate determination and in development, one can further envision complex autonomous sense-and-respond circuits that monitor and control cell fate in diverse scenarios such as stem cell therapy, artificial developmental schemes, and tissue engineering and regeneration.

EXPERIMENTAL PROCEDURES

For details, see Supplemental Experimental Procedures. Briefly, plasmids were constructed using standard restriction-ligation cloning. cDNA of mammalian TFs was obtained from the Integrated Molecular Analysis of Genomes and their Expression (IMAGE) Consortium. All plasmids were purified with an endotoxin removal kit (Norgen) before transfection. Cell lines were obtained commercially and cultured using recommended media for up to 2 months. Transfections were done using Lipofectamine 2000 (Life Technologies) according to guidelines. Transfection setup and the scale for each panel are reported in Table S4. Microscopy images were taken ~48 hr post-transfection using a Nikon Eclipse Ti inverted microscope. Appropriate filter combinations were used to image different fluorescent proteins. Flow cytometry measurements were performed ~48 hr post-transfection on a BD Biosciences LSRFortessa II cell analyzer. Photomultiplier tube (PMT) voltage in the AmCyan channel was different between open-loop and feedback sensors, and a conversion factor was calculated to bring the readouts to the same scale (Figures S2A and S2B). Data analysis for bar charts was performed with FlowJo software. The model was built with SimBiology and binning, and data fitting was done with MATLAB.

SUPPLEMENTAL INFORMATION

Supplemental Information includes Supplemental Experimental Procedures, six figures, and four tables and can be found with this article online at http://dx.doi.org/10.1016/j.celrep.2016.07.061.

AUTHOR CONTRIBUTIONS

B.A. conceived the project, performed most experiments, analyzed the data, and wrote the paper. E.M. and B.H. performed some experiments. Y.B. conceived the project, analyzed the data, wrote the paper, and supervised the project.

ACKNOWLEDGMENTS

The research was funded by ERC StG 281490 (CellControl). We thank T. Horn and V. Jaeggin for help with flow cytometry, Y.B. lab members for discussions, and the M. Fussenegger lab for PIT2 and ET constructs.

Received: January 4, 2016
Revised: June 19, 2016
Accepted: July 22, 2016
Published: August 18, 2016

Figure 7. Transduction of Transcriptional Activity into Various Downstream Processes

(A) Multipronged actuation combining downstream RNAi with transactivation, including a low-leakage RNAi target with recombinase delay and a transactivation target, PIR-driven mCitrine.

(B) The improvement in RNAi knockdown with the delayed switch, comparing between on and off mCherry readouts in the delayed and standard configurations (top) and flow cytometry plots (bottom).

(C) The outputs generated by the multipronged sensor in three cell lines triggered by the endogenous HNF1A/B activation. The rows show representative images of AmCyan (cyan), Citrine (yellow), and mCherry (red). Transfection marker infrared fluorescent protein (iRFP; purple) is in a separate row. Scale bars, 100 μm. Note the low transfection efficiency in HeLa cells.

(D) Schematics of TF-driven, feedback-amplified expression of Cre recombinase.

(E) Response of two amplified Cre sensors to ectopic induction of their respective cognate TF (HNF1A and SOX10) (left) and corresponding flow cytometry plots (right).

(F) Endogenous TF-driven, recombinase-triggered gene inversion in three cell lines. The figure shows the response of the sensor for HNF1A/B (top) and SOX9/10 (bottom). Representative images are shown. The Citrine signal (yellow) is represented over the corresponding image for the iRFP transfection marker (purple). Scale bars, 100 μm. HeLa cell images have higher background when similar settings are applied to all images in this panel.

In (B), (C), (E), and (F), each bar represents mean ± SD of biological triplicates.

REFERENCES

Acar, M., Becskei, A., and van Oudenaarden, A. (2005). Enhancement of cellular memory by reducing stochastic transitions. Nature *435*, 228–232.

Ajo-Franklin, C.M., Drubin, D.A., Eskin, J.A., Gee, E.P.S., Landgraf, D., Phillips, I., and Silver, P.A. (2007). Rational design of memory in eukaryotic cells. Genes Dev. *21*, 2271–2276.

Alon, U. (2007). Network motifs: theory and experimental approaches. Nat. Rev. Genet. *8*, 450–461.

Amit, R., Garcia, H.G., Phillips, R., and Fraser, S.E. (2011). Building enhancers from the ground up: a synthetic biology approach. Cell *146*, 105–118.

Ausländer, S., Ausländer, D., Müller, M., Wieland, M., and Fussenegger, M. (2012). Programmable single-cell mammalian biocomputers. Nature *487*, 123–127.

Ausländer, D., Ausländer, S., Charpin-El Hamri, G., Sedlmayer, F., Müller, M., Frey, O., Hierlemann, A., Stelling, J., and Fussenegger, M. (2014). A synthetic multifunctional mammalian pH sensor and CO2 transgene-control device. Mol. Cell *55*, 397–408.

Becskei, A., Séraphin, B., and Serrano, L. (2001). Positive feedback in eukaryotic gene networks: cell differentiation by graded to binary response conversion. EMBO J. *20*, 2528–2535.

Benenson, Y. (2012). Biomolecular computing systems: principles, progress and potential. Nat. Rev. Genet. *13*, 455–468.

Bleris, L., Xie, Z., Glass, D., Adadey, A., Sontag, E., and Benenson, Y. (2011). Synthetic incoherent feedforward circuits show adaptation to the amount of their genetic template. Mol. Syst. Biol. *7*, 519.

Boj, S.F., Parrizas, M., Maestro, M.A., and Ferrer, J. (2001). A transcription factor regulatory circuit in differentiated pancreatic cells. Proc. Natl. Acad. Sci. USA *98*, 14481–14486.

Briançon, N., Bailly, A., Clotman, F., Jacquemin, P., Lemaigre, F.P., and Weiss, M.C. (2004). Expression of the alpha7 isoform of hepatocyte nuclear factor (HNF) 4 is activated by HNF6/OC-2 and HNF1 and repressed by HNF4alpha1 in the liver. J. Biol. Chem. *279*, 33398–33408.

Buckley, S.M., Delhove, J.M., Perocheau, D.P., Karda, R., Rahim, A.A., Howe, S.J., Ward, N.J., Birrell, M.A., Belvisi, M.G., Arbuthnot, P., et al. (2015). In vivo bioimaging with tissue-specific transcription factor activated luciferase reporters. Sci. Rep. *5*, 11842.

Busskamp, V., Duebel, J., Balya, D., Fradot, M., Viney, T.J., Siegert, S., Groner, A.C., Cabuy, E., Forster, V., Seeliger, M., et al. (2010). Genetic reactivation of cone photoreceptors restores visual responses in retinitis pigmentosa. Science *329*, 413–417.

Cruz-Solis, I., Zepeda, R.C., Ortiz, S., Aguilera, J., López-Bayghen, E., and Ortega, A. (2009). Glutamate-dependent transcriptional control in Bergmann glia: Sox10 as a repressor. J. Neurochem. *109*, 899–910.

Culler, S.J., Hoff, K.G., and Smolke, C.D. (2010). Reprogramming cellular behavior with RNA controllers responsive to endogenous proteins. Science *330*, 1251–1255.

Dean, S., Tang, J.I., Seckl, J.R., and Nyirenda, M.J. (2010). Developmental and tissue-specific regulation of hepatocyte nuclear factor 4-alpha (HNF4-alpha) isoforms in rodents. Gene Expr. *14*, 337–344.

Deans, T.L., Cantor, C.R., and Collins, J.J. (2007). A tunable genetic switch based on RNAi and repressor proteins for regulating gene expression in mammalian cells. Cell *130*, 363–372.

Elowitz, M.B., and Leibler, S. (2000). A synthetic oscillatory network of transcriptional regulators. Nature *403*, 335–338.

Enciso, G., and Sontag, E.D. (2005). Monotone systems under positive feedback: multistability and a reduction theorem. Syst. Control Lett. *54*, 159–168.

Fang, B., Mane-Padros, D., Bolotin, E., Jiang, T., and Sladek, F.M. (2012). Identification of a binding motif specific to HNF4 by comparative analysis of multiple nuclear receptors. Nucleic Acids Res. *40*, 5343–5356.

Farzadfard, F., Perli, S.D., and Lu, T.K. (2013). Tunable and multifunctional eukaryotic transcription factors based on CRISPR/Cas. ACS Synth. Biol. *2*, 604–613.

Fiering, S., Northrop, J.P., Nolan, G.P., Mattila, P.S., Crabtree, G.R., and Herzenberg, L.A. (1990). Single cell assay of a transcription factor reveals a threshold in transcription activated by signals emanating from the T-cell antigen receptor. Genes Dev. *4*, 1823–1834.

Fire, A., Xu, S., Montgomery, M.K., Kostas, S.A., Driver, S.E., and Mello, C.C. (1998). Potent and specific genetic interference by double-stranded RNA in *Caenorhabditis elegans*. Nature *391*, 806–811.

Friedland, A.E., Lu, T.K., Wang, X., Shi, D., Church, G., and Collins, J.J. (2009). Synthetic gene networks that count. Science *324*, 1199–1202.

Fussenegger, M., Morris, R.P., Fux, C., Rimann, M., von Stockar, B., Thompson, C.J., and Bailey, J.E. (2000). Streptogramin-based gene regulation systems for mammalian cells. Nat. Biotechnol. *18*, 1203–1208.

Gardner, T.S., Cantor, C.R., and Collins, J.J. (2000). Construction of a genetic toggle switch in *Escherichia coli*. Nature *403*, 339–342.

Green, A.A., Silver, P.A., Collins, J.J., and Yin, P. (2014). Toehold switches: de-novo-designed regulators of gene expression. Cell *159*, 925–939.

Halpern, M.E., Rhee, J., Goll, M.G., Akitake, C.M., Parsons, M., and Leach, S.D. (2008). Gal4/UAS transgenic tools and their application to zebrafish. Zebrafish *5*, 97–110.

Hansen, J., Mailand, E., Swaminathan, K.K., Schreiber, J., Angelici, B., and Benenson, Y. (2014). Transplantation of prokaryotic two-component signaling pathways into mammalian cells. Proc. Natl. Acad. Sci. USA *111*, 15705–15710.

Hobert, O. (2008). Gene regulation by transcription factors and microRNAs. Science *319*, 1785–1786.

Janknecht, R., Ernst, W.H., Pingoud, V., and Nordheim, A. (1993). Activation of ternary complex factor Elk-1 by MAP kinases. EMBO J. *12*, 5097–5104.

Jolma, A., Yan, J., Whitington, T., Toivonen, J., Nitta, K.R., Rastas, P., Morgunova, E., Enge, M., Taipale, M., Wei, G., et al. (2013). DNA-binding specificities of human transcription factors. Cell *152*, 327–339.

Kadaja, M., Keyes, B.E., Lin, M., Pasolli, H.A., Genander, M., Polak, L., Stokes, N., Zheng, D., and Fuchs, E. (2014). SOX9: a stem cell transcriptional regulator of secreted niche signaling factors. Genes Dev. *28*, 328–341.

Kadonaga, J.T., Carner, K.R., Masiarz, F.R., and Tjian, R. (1987). Isolation of cDNA encoding transcription factor Sp1 and functional analysis of the DNA binding domain. Cell *51*, 1079–1090.

Khalil, A.S., Lu, T.K., Bashor, C.J., Ramirez, C.L., Pyenson, N.C., Joung, J.K., and Collins, J.J. (2012). A synthetic biology framework for programming eukaryotic transcription functions. Cell *150*, 647–658.

Kikuchi, R., Kusuhara, H., Hattori, N., Kim, I., Shiota, K., Gonzalez, F.J., and Sugiyama, Y. (2007). Regulation of tissue-specific expression of the human and mouse urate transporter 1 gene by hepatocyte nuclear factor 1 alpha/beta and DNA methylation. Mol. Pharmacol. *72*, 1619–1625.

Kim, H.D., and O'Shea, E.K. (2008). A quantitative model of transcription factor-activated gene expression. Nat. Struct. Mol. Biol. *15*, 1192–1198.

Kitanaka, S., Sato, U., and Igarashi, T. (2007). Regulation of human insulin, IGF-I, and multidrug resistance protein 2 promoter activity by hepatocyte nuclear factor (HNF)-1beta and HNF-1alpha and the abnormality of HNF-1beta mutants. J. Endocrinol. *192*, 141–147.

Kobayashi, H., Kaern, M., Araki, M., Chung, K., Gardner, T.S., Cantor, C.R., and Collins, J.J. (2004). Programmable cells: interfacing natural and engineered gene networks. Proc. Natl. Acad. Sci. USA *101*, 8414–8419.

Küspert, M., Weider, M., Müller, J., Hermans-Borgmeyer, I., Meijer, D., and Wegner, M. (2012). Desert hedgehog links transcription factor Sox10 to perineurial development. J. Neurosci. *32*, 5472–5480.

Lapique, N., and Benenson, Y. (2014). Digital switching in a biosensor circuit via programmable timing of gene availability. Nat. Chem. Biol. *10*, 1020–1027.

Leisner, M., Bleris, L., Lohmueller, J., Xie, Z., and Benenson, Y. (2010). Rationally designed logic integration of regulatory signals in mammalian cells. Nat. Nanotechnol. *5*, 666–670.

Li, Y., Jiang, Y., Chen, H., Liao, W., Li, Z., Weiss, R., and Xie, Z. (2015). Modular construction of mammalian gene circuits using TALE transcriptional repressors. Nat. Chem. Biol. *11*, 207–213.

Lienert, F., Torella, J.P., Chen, J.H., Norsworthy, M., Richardson, R.R., and Silver, P.A. (2013). Two- and three-input TALE-based AND logic computation in embryonic stem cells. Nucleic Acids Res. *41*, 9967–9975.

Lin, Y.S., Carey, M., Ptashne, M., and Green, M.R. (1990). How different eukaryotic transcriptional activators can cooperate promiscuously. Nature *345*, 359–361.

Lucas, B., Grigo, K., Erdmann, S., Lausen, J., Klein-Hitpass, L., and Ryffel, G.U. (2005). HNF4alpha reduces proliferation of kidney cells and affects genes deregulated in renal cell carcinoma. Oncogene *24*, 6418–6431.

Maeder, M.L., Linder, S.J., Reyon, D., Angstman, J.F., Fu, Y., Sander, J.D., and Joung, J.K. (2013). Robust, synergistic regulation of human gene expression using TALE activators. Nat. Methods *10*, 243–245.

McManus, M.T., and Sharp, P.A. (2002). Gene silencing in mammals by small interfering RNAs. Nat. Rev. Genet. *3*, 737–747.

Nissim, L., and Bar-Ziv, R.H. (2010). A tunable dual-promoter integrator for targeting of cancer cells. Mol. Syst. Biol. *6*, 444.

Odom, D.T., Zizlsperger, N., Gordon, D.B., Bell, G.W., Rinaldi, N.J., Murray, H.L., Volkert, T.L., Schreiber, J., Rolfe, P.A., Gifford, D.K., et al. (2004). Control of pancreas and liver gene expression by HNF transcription factors. Science *303*, 1378–1381.

Olson, E.J., Hartsough, L.A., Landry, B.P., Shroff, R., and Tabor, J.J. (2014). Characterizing bacterial gene circuit dynamics with optically programmed gene expression signals. Nat. Methods *11*, 449–455.

Park, S.H., Zarrinpar, A., and Lim, W.A. (2003). Rewiring MAP kinase pathways using alternative scaffold assembly mechanisms. Science *299*, 1061–1064.

Patwardhan, R.P., Hiatt, J.B., Witten, D.M., Kim, M.J., Smith, R.P., May, D., Lee, C., Andrie, J.M., Lee, S.I., Cooper, G.M., et al. (2012). Massively parallel functional dissection of mammalian enhancers in vivo. Nat. Biotechnol. *30*, 265–270.

Peirano, R.I., and Wegner, M. (2000). The glial transcription factor Sox10 binds to DNA both as monomer and dimer with different functional consequences. Nucleic Acids Res. *28*, 3047–3055.

Perez-Pinera, P., Ousterout, D.G., Brunger, J.M., Farin, A.M., Glass, K.A., Guilak, F., Crawford, G.E., Hartemink, A.J., and Gersbach, C.A. (2013). Synergistic and tunable human gene activation by combinations of synthetic transcription factors. Nat. Methods *10*, 239–242.

Prochazka, L., Angelici, B., Haefliger, B., and Benenson, Y. (2014). Highly modular bow-tie gene circuits with programmable dynamic behaviour. Nat. Commun. *5*, 4729.

Ran, T., Douek, Y., Milo, L., and Shapiro, E. (2012). A programmable NOR-based device for transcription profile analysis. Sci. Rep. *2*, 641.

Rinaudo, K., Bleris, L., Maddamsetti, R., Subramanian, S., Weiss, R., and Benenson, Y. (2007). A universal RNAi-based logic evaluator that operates in mammalian cells. Nat. Biotechnol. *25*, 795–801.

Rosenfeld, N., Young, J.W., Alon, U., Swain, P.S., and Elowitz, M.B. (2005). Gene regulation at the single-cell level. Science *307*, 1962–1965.

Schödel, J., Oikonomopoulos, S., Ragoussis, J., Pugh, C.W., Ratcliffe, P.J., and Mole, D.R. (2011). High-resolution genome-wide mapping of HIF-binding sites by ChIP-seq. Blood *117*, e207–e217.

Senkel, S., Lucas, B., Klein-Hitpass, L., and Ryffel, G.U. (2005). Identification of target genes of the transcription factor HNF1beta and HNF1alpha in a human embryonic kidney cell line. Biochim. Biophys. Acta *1731*, 179–190.

Sharon, E., Kalma, Y., Sharp, A., Raveh-Sadka, T., Levo, M., Zeevi, D., Keren, L., Yakhini, Z., Weinberger, A., and Segal, E. (2012). Inferring gene regulatory logic from high-throughput measurements of thousands of systematically designed promoters. Nat. Biotechnol. *30*, 521–530.

Slomovic, S., and Collins, J.J. (2015). DNA sense-and-respond protein modules for mammalian cells. Nat. Methods *12*, 1085–1090.

Smith, R.P., Taher, L., Patwardhan, R.P., Kim, M.J., Inoue, F., Shendure, J., Ovcharenko, I., and Ahituv, N. (2013). Massively parallel decoding of mammalian regulatory sequences supports a flexible organizational model. Nat. Genet. *45*, 1021–1028.

Steen, E.J., Kang, Y., Bokinsky, G., Hu, Z., Schirmer, A., McClure, A., Del Cardayre, S.B., and Keasling, J.D. (2010). Microbial production of fatty-acid-derived fuels and chemicals from plant biomass. Nature *463*, 559–562.

Stricker, J., Cookson, S., Bennett, M.R., Mather, W.H., Tsimring, L.S., and Hasty, J. (2008). A fast, robust and tunable synthetic gene oscillator. Nature *456*, 516–519.

Tamsir, A., Tabor, J.J., and Voigt, C.A. (2011). Robust multicellular computing using genetically encoded NOR gates and chemical "wires.". Nature *469*, 212–215.

Tan, C., Marguet, P., and You, L. (2009). Emergent bistability by a growth-modulating positive feedback circuit. Nat. Chem. Biol. *5*, 842–848.

Thomas, H., Jaschkowitz, K., Bulman, M., Frayling, T.M., Mitchell, S.M., Roosen, S., Lingott-Frieg, A., Tack, C.J., Ellard, S., Ryffel, G.U., and Hattersley, A.T. (2001). A distant upstream promoter of the HNF-4alpha gene connects the transcription factors involved in maturity-onset diabetes of the young. Hum. Mol. Genet. *10*, 2089–2097.

Tigges, M., Marquez-Lago, T.T., Stelling, J., and Fussenegger, M. (2009). A tunable synthetic mammalian oscillator. Nature *457*, 309–312.

Tronche, F., Ringeisen, F., Blumenfeld, M., Yaniv, M., and Pontoglio, M. (1997). Analysis of the distribution of binding sites for a tissue-specific transcription factor in the vertebrate genome. J. Mol. Biol. *266*, 231–245.

Veeman, M.T., Slusarski, D.C., Kaykas, A., Louie, S.H., and Moon, R.T. (2003). Zebrafish prickle, a modulator of noncanonical Wnt/Fz signaling, regulates gastrulation movements. Curr. Biol. *13*, 680–685.

Weber, W., Fux, C., Daoud-el Baba, M., Keller, B., Weber, C.C., Kramer, B.P., Heinzen, C., Aubel, D., Bailey, J.E., and Fussenegger, M. (2002). Macrolide-based transgene control in mammalian cells and mice. Nat. Biotechnol. *20*, 901–907.

Wegner, M. (2010). All purpose Sox: The many roles of Sox proteins in gene expression. Int. J. Biochem. Cell Biol. *42*, 381–390.

Wissmüller, S., Kosian, T., Wolf, M., Finzsch, M., and Wegner, M. (2006). The high-mobility-group domain of Sox proteins interacts with DNA-binding domains of many transcription factors. Nucleic Acids Res. *34*, 1735–1744.

Xie, Z., Wroblewska, L., Prochazka, L., Weiss, R., and Benenson, Y. (2011). Multi-input RNAi-based logic circuit for identification of specific cancer cells. Science *333*, 1307–1311.

Xiong, W., and Ferrell, J.E., Jr. (2003). A positive-feedback-based bistable "memory module" that governs a cell fate decision. Nature *426*, 460–465.

Zhang, Q., and Andersen, M.E. (2007). Dose response relationship in anti-stress gene regulatory networks. PLoS Comput. Biol. *3*, e24.

Zhou, D., Bai, F., Zhang, X., Hu, M., Zhao, G., Zhao, Z., and Liu, R. (2014). SOX10 is a novel oncogene in hepatocellular carcinoma through Wnt/β-catenin/TCF4 cascade. Tumour Biol. *35*, 9935–9940.

Cell Reports, Volume *16*

Supplemental Information

Synthetic Biology Platform for Sensing and Integrating Endogenous Transcriptional Inputs in Mammalian Cells

Bartolomeo Angelici, Erik Mailand, Benjamin Haefliger, and Yaakov Benenson

Supplemental Figure Titles and Legends

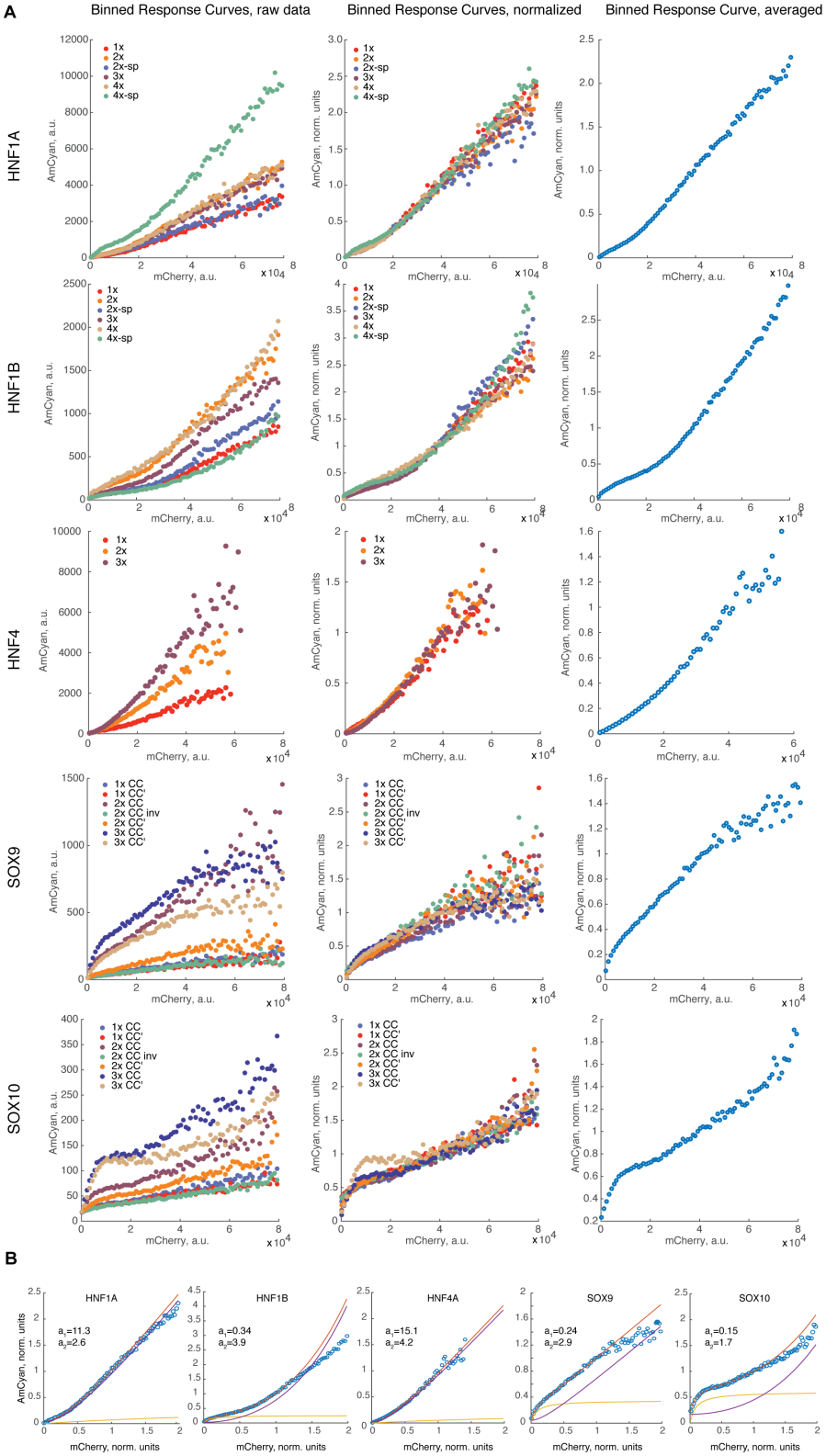

Figure S1. Related to Figure 1. (**A**) Fine binning of the response curves of open-loop TF sensors. Left to right, individual REs' response curves; curves normalized to output expression in the 40th bin (40,000 arbitrary flow cytometry units); averaged normalized curve. Transcription factors and individual response elements are indicated. (**B**) Deconvolution of

the open-loop response curves into a quadratic-linear (purple curve) and a saturating response (brown curve). The sum of the responses is a red curve. The fitted parameters of the saturating component are shown (a_1, the "IC50"; a_2, saturation level, in arbitrary units)

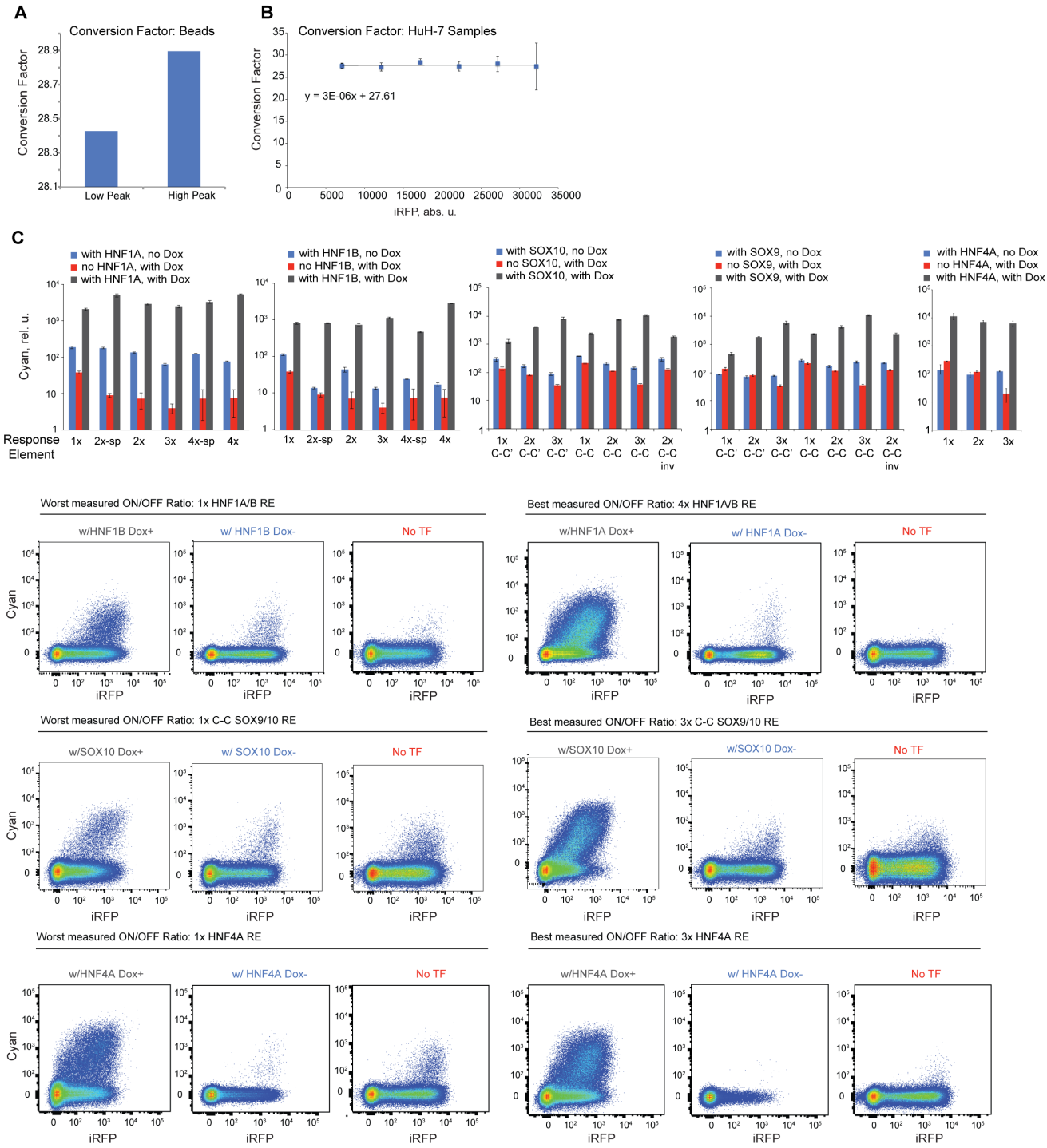

Figure S2. Related to Figure 2. **(A,B)** Calculating the conversion factor between different flow cytometer settings for comparing open-loop and feedback sensors. **(A)** Conversion factor calculated using SPHERO RainBow Calibration particles measured with photomultiplier voltages of 250V and 400V, respectively, and filter settings corresponding to AmCyan readout. The bars show the ratio between fluorescence units measured using the two settings. **(B)** The conversion factor calculated using the same samples measured with different PMT voltages. The dots and the linear regression show the conversion factor (AmCyan at PMT voltage of 400V/AmCyan at PMT voltage of 250V) as a function of iRFP transfection control intensity (measured using constant PMT settings), error bars represents s.d. of three biological replicates. **(C)** The feedback-amplified outputs in HEK293 Tet-On cells in the presence of ectopic TFs compared to the background expression without Dox (but with the ectopic cassette) and the background measured in the absence of TF-encoding gene. The bar charts summarize the data for all the response elements for the five transcription factors. Each bar represents mean±s.d. of three biological replicates. Below, flow cytometry plots show the best and the worst cases for each Transcription Factor family.

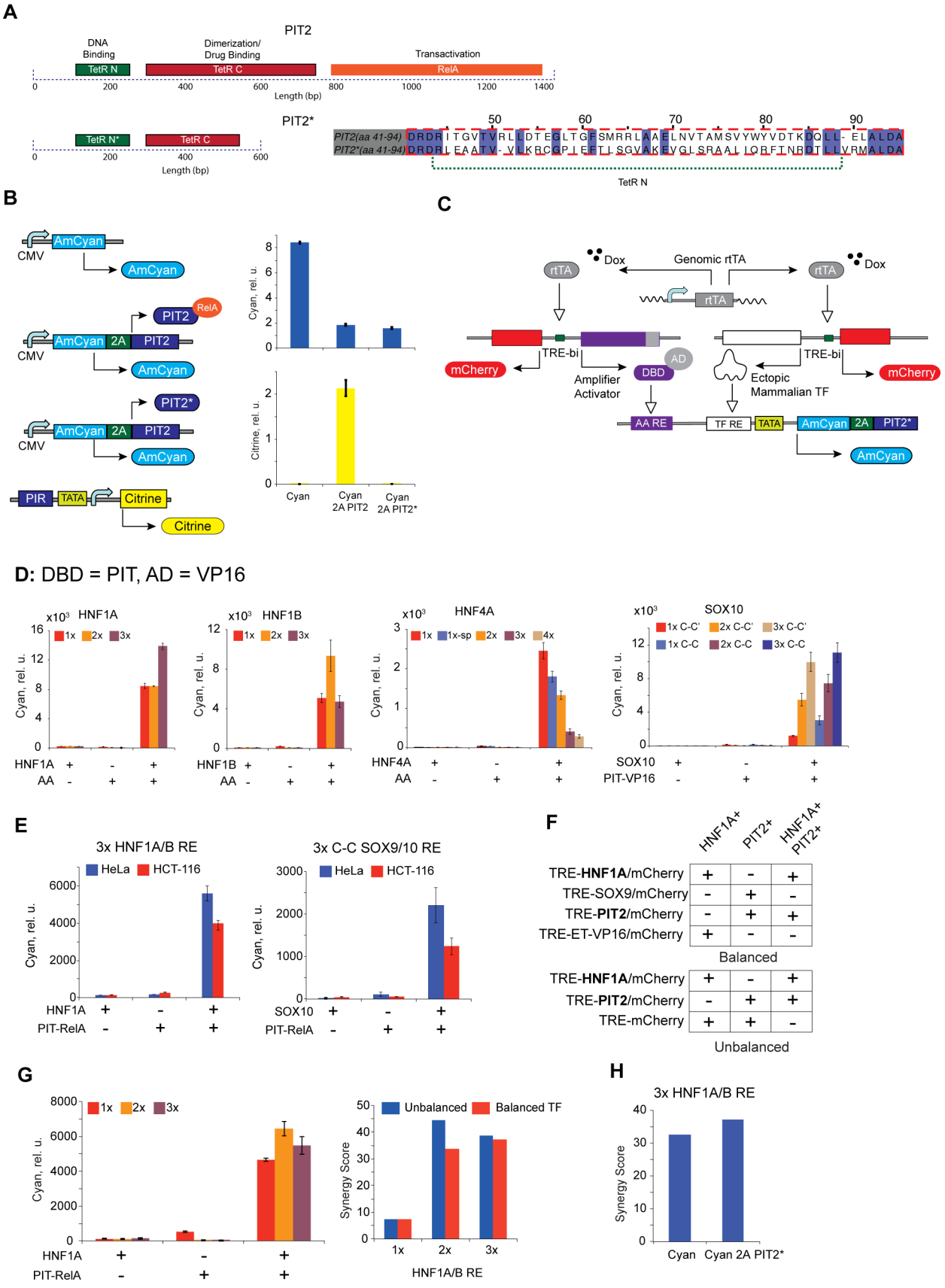

Figure S3. Related to Figure 3. (**A,B**) Evaluation of PIT2 loss-of-function mutant and the effect of 2A linker on gene expression. (**A**) Schematics of mutation in the PIT2 gene. We swap the DNA binding domain with the one derived from the ET transcriptional regulator, and preserve the rest of the sequence in order to enable direct comparison to the readouts

of feedback circuits. The resulting mutant protein PIT2* has high sequence homology with the original PIT2 but is unable to bind DNA due to the mismatch between its binding and dimerization domains. We also delete the transactivation domain. (**B**) Funcitonal evaluation of PIT2 mutant. Left, constructs used in the experiment. Various AmCyan-driving constructs (not coupled to PIT2, coupled to PIT2 via 2A linker, and coupled to PIT2 mutant via 2A linker) are contransfectd with the PIR-Citrine reporter. Only the AmCyan-2A-PIT2 is able to transactivate the reporter. Note that the AmCyan intensity drops 5-fold due to the 2A linker introduction. Each bar represents mean±s.d. of three biological replicates. (**C-H**) Data related to synergy measurements (**C**) Detailed schematics of the synergy measurements. Both the TF of interest and the amplifier activators are controlled via TRE promoters, and each is coexpressed with mCherry reporter. For partial activation conditions (TF only or AA only), the omitted activator is replaced with a similar construct expressing mCherry and a "balancing" factor that does not bind to the composite promoter. (**D**) The effect of replacing the transactivation domain of the amplifying activator from RelA to VP16. Top, different transcriptional complexes are shown. The bar charts' layout is similar to that in Figure 3 C. Each bar represents mean±s.d. of three biological replicates. (**E**) Synergy measurements in two additional cell lines, HeLa and HCT-116. The response elements and TF inputs are indicated. CMV-rtTA was transfected into the cell lines to enable Dox-controleld induction of TRE-TF and TRE-AA constructs. Each bar represents mean±s.d. of three biological replicates. (**F**) Plasmid mixtures used to produce the different combinations of transcriptional inputs for the Balanced and the Unbalanced cases. Shorthand notations of the constructs are indicated, with TRE-X/Y meaning a bidirectional TRE promoter expressing genes X and Y. (**G**) Synergy measurements for the Unbalanced setup. Left, expression levels reached with either, or both, transcriptional inputs provided to the composite promoters containing HNF1A response elements in the Unbalanced transfection setup. Each bar represents mean±s.d. of three biological replicates. Right, comparison of the synergy scores of the same composite promotersin the Balanced and Unbalanced setups. (**H**) Comparison of the measured synergy scores between two HNF1A/B composite promoter driving, respectively, the expression of the Cyan fluorescent protein alone or the mutated feedback loop (Cyan 2A PIT2*). We use PIR::3x-HNF1A/B RE composite promoter because it has the highest synergy in the original dataset.

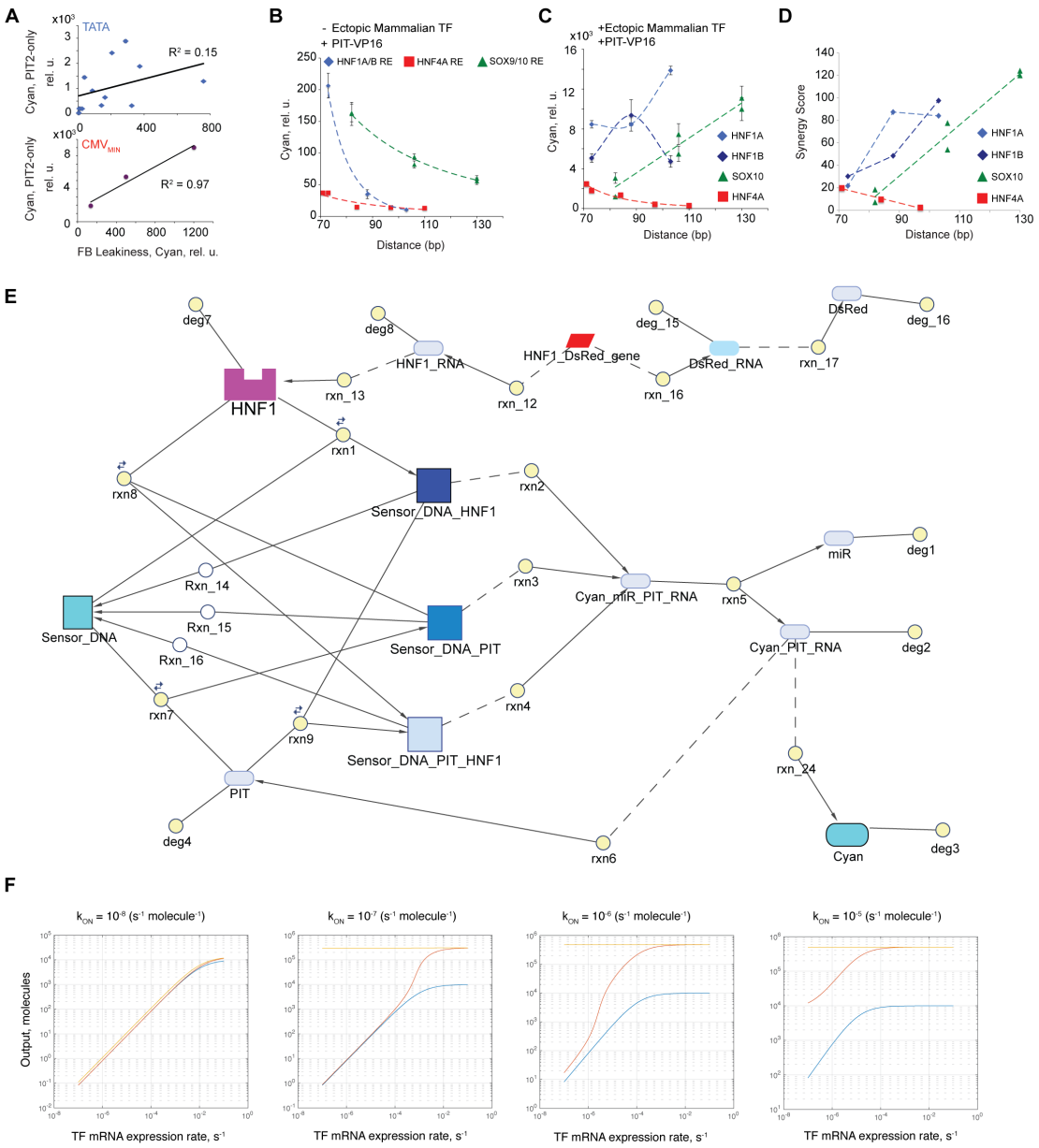

Figure S4. Related to Figure 4. (**A**) The relationship between the intrinsic sensor leakiness as measured with feedback-amplified sensors in the absence of the input TF, and the transactivation efficiency of the amplifier activator alone. Top, all sensors that employ minimal TATA box; bottom, sensors employing CMV_{MIN}. (**B**) Transactivating efficiency of PIT-VP16 amplifier activator alone, as a function of PIR distance from the TATA box. Error bars represent s.d. of three biological replicates (**C**) Fully induced expression levels from a composite promoter achieved by providing both the indicated ectopic TF input and the amplifier activator PIT-VP16 (synergized expression). Error bars represent s.d. of three biological replicates. (**D**) Synergy scores for different composite promoters with PIT-VP16 as amplifier activator as a function of PIR distance from the TATA box. (**E**) The model created in SimBiology to simulate the synergistic amplified loop. (**F**) Simulation results showing the outputs of the open loop, synergistic amplified loop, and an amplified loop without synergy as a function of TF expression rate. The charts are simulated for different values of TF binding rate constant K_{ON} as indicated.

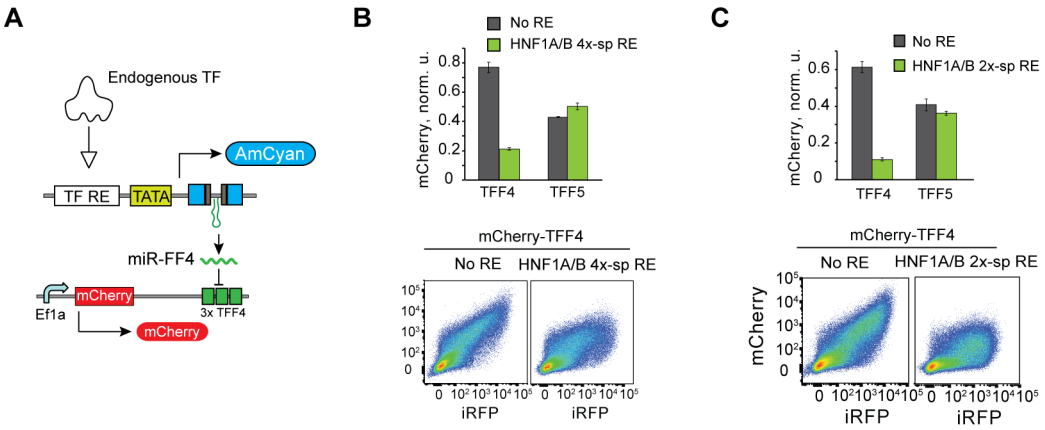

Figure S5. Related to Fig. 7. (**A**) The schematics of TF-induced RNAi. (**B**) Bulk effects and representative flow cytometry plots of mCherry fluorescence in the absence and the presence of a sensor in HuH-7 cells. TFF4 and TFF5 indicate constitutive mCherry constructs fused with these targets. TFF5 is not targeted by miR-FF4. (**C**) RNAi induced by the amplified HNF1A/B 2x-sp RE sensor in HuH-7 cells. Bulk comparison is at the top with representative flow cytometry scatter plots shown below. iRFP serves as a transfection marker. In panels **B** and **C** each bar represents mean±s.d. of three biological replicates

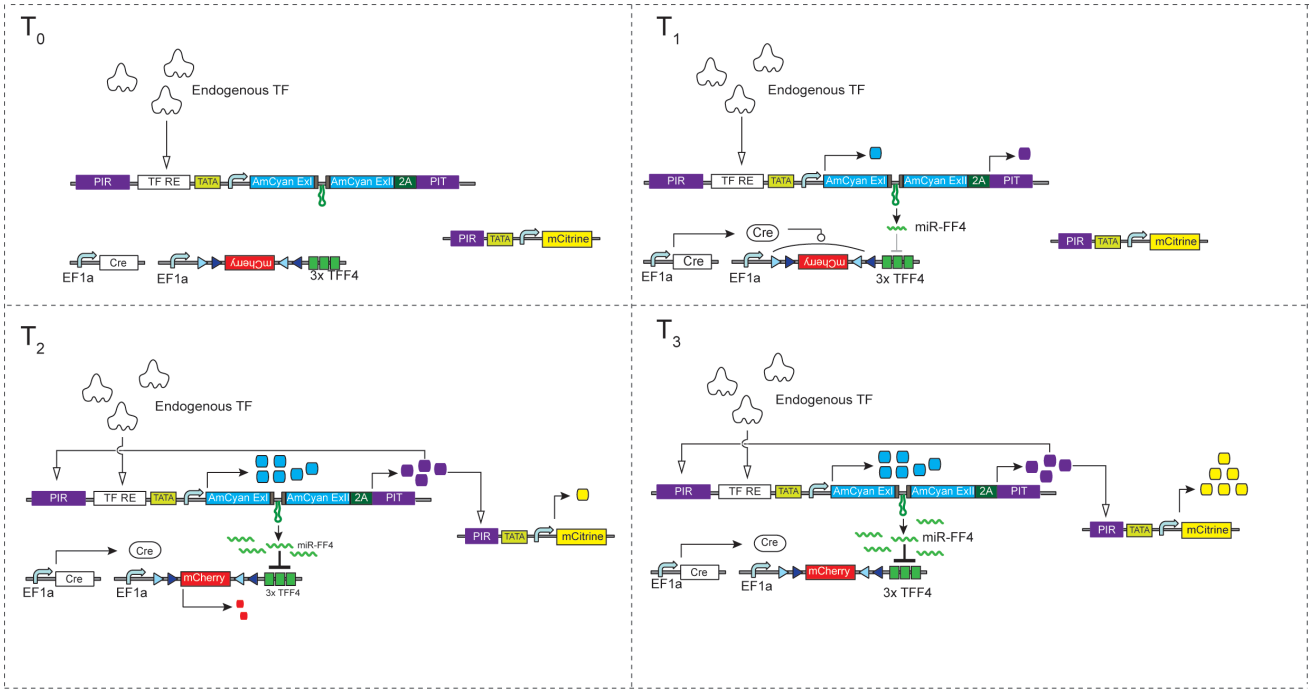

Figure S6. Related to Fig. 7. Schematic representation of the multipronged actuation circuit dynamics. The continuous process is broken down in four separate phases for clarity. In each phase the number of colored boxes is a visual representation of the relative protein concentration and the presence of arrows indicates reactions taking place at a meaningful rate in the specific phase: transcriptional regulation at the promoter level (open arrows), translation or post-transcriptional modifications (solid arrows) and DNA inversion (circular arrowhead).

Supplemental Tables

Table S1. Related to Figure 2. Quantitative outputs with feedback-amplified sensors and the background expression. The values are factored to be directly comparable with open-loop values.

Ectopic TF	Sensor	+TF/+Dox	+TF/-Dox	-TF/+Dox	On/Off Ratio
HNF1A	1x	2053.13	184.39	38.03	54
	2x-sp	4948.82	177.22	8.97	552
	2x	2885.65	132.87	7.13	405
	3x	2440.62	62.94	3.98	613
	4x-sp	3248.16	122.53	7.29	446
	4x	5198.07	75.00	7.44	699
HNF1B	1x	803.61	111.25	38.03	21
	2x-sp	813.16	13.65	8.97	91
	2x	727.66	43.38	7.13	102
	3x	1141.45	13.37	3.98	287
	4x-sp	467.25	23.92	7.29	64
	4x	2820.24	16.95	7.44	379
SOX9	1x C-C’	1234.81	287.41	134.65	9
	2x C-C’	4029.96	162.72	80.75	50
	3x C-C’	8222.87	86.22	34.59	238
	1x C-C	2343.46	373.45	211.67	11
	2x C-C	7290.15	205.02	113.95	64
	3x C-C	10600.37	141.50	36.14	293
	2x C-C inv	1758.33	287.18	123.26	14
SOX10	1x C-C’	465.67	87.75	134.65	3
	2x C-C’	1787.43	70.08	80.75	22
	3x C-C’	5819.88	77.63	34.59	168
	1x C-C	2369.78	267.77	211.67	11
	2x C-C	4146.43	164.64	113.95	36
	3x C-C	10729.40	239.97	36.14	297
	2x C-C inv	2300.66	218.45	123.26	19
HNF4A	1x	11398.15	136.26	283.59	40
	2x	7188.26	92.91	119.68	60
	3x	6319.61	122.29	19.94	317

Table S2. Related to Figure 5. Quantitative outputs with feedback-amplified sensors and corresponding background expression. The specific conditions of induction for each TF are described above in **Forward design of amplified sensors**. The values are factored to be directly comparable with open-loop values.

TF	Sensor	Induced	Non Induced	On/Off Ratio
HIF1A	1x	12910.06	352.51	16
	2x	7644.67	247.50	29
	3x	9168.04	140.15	48
TCF/LEF	1x	3233.7	20.3	159
	3x	7629.3	41.3	185
	6x	3950.4	29.1	136
CA-NFATC1	1x	12910.06	76.60	169
	2x	7644.67	42.70	179
	3x	9168.04	29.54	310

Table S3. Related to Material and Methods. Oligonucleotide and gBlock sequences used for cloning.

Primer name	Sequence 5' → 3'
PR0121	CGCGCCAGTTAATAATTAACTTAGCGCCGGCAGTTAATAATTAACTTCCATATGCTCTAG AGGGTATATAATGGGGGCCA
PR0122	CTAGTGGCCCCCATTATATACCCTCTAGAGCATATGGAAGTTAATTATTAACT GCCGGCGCTAAGTTAATTATTAACTGG
PR0123	CGCGCCAGTTAATAATTAACTTAGCGCCGGCAGTTAATAATTAACTTAGCGCCGGCAGTT AATAATTAACTTAGCGCCGGCAGTTAATAATTAACTCA
PR0124	TATGAGTTAATTATTAACTGCCGGCGCTAAGTTAATTATTAACTGCCGGCGCTAAGTTAA TTATTAACTGCCGGCGCTAAGTTAATTATTAACTGG
PR0125	TCAATTACTAGTCTACTACCAGAGCTCATCGCTAG
PR0126	CTATTGGCGCGCCCCCGTAGCTTGGCGTAATCA
PR0604	CGCGCCAGTTAATAATTAACTAGTTAATAATTAACTCA
PR0605	TATGAGTTAATTATTAACTAGTTAATTATTAACTGG
PR0606	CGCGCCAGTTAATAATTAACTAGTTAATAATTAACTAGTTAATAATTAACTCA
PR0607	TATGAGTTAATTATTAACTAGTTAATTATTAACTAGTTAATTATTAACTGG
BA 1.68.3	CGCGCCAGTTAATAATTAACTAGTTAATAATTAACTAGTTAATAATTAACTAGTTAATAA TTAACTCA
BA 1.68.4	TATGAGTTAATTATTAACTAGTTAATTATTAACTAGTTAATTATTAACTAGTTAATTATTA ACTGG
PR0387	CTCTACAGATCTATGAGTCGAGGAGAGGTGCG
PR0388	GAGAGTAAGCTTTCCTTAGGAGCTGATCTGACTCA
PR0421	CATGTGAAATAGCGCTGTACAGCGTATGGGAATCTCTTGTACGGTGTACGAGTATCTTCC CGTACACCGTACGG
PR0422	CGCGCCGTACGGTGTACGGGAAGATACTCGTACACCGTACAAGAGATTCCCATACGCTG TACAGCGCTATTTCA
PR0431	CCGGAAGAGCCGAGGGCAGGGGAAGTCTTCTAACATGCGGGGACGTGGAGGAAAATCC CGGGCCCA
PR0432	GATCTGGGCCCGGGATTTTCCTCCACGTCCCCGCATGTTAGAAGACTTCCCCTGCCCTCG GCTCTT
PR0700	CATCCTGCGGCCGCCATTTCCCCGAAAAGTGCCACC
PR0702	CATCCTAAGCTTGCTACTTGTACAGCTCGTCCATGC
PR1012	GCCACGGGCGCGCCGCTAGAGCTCGCGGTGCCGAATTCT
PR1013	GGAGCAGGTACCGTCGACTGCAGAATTCG
PR1402	GCAGCGGCTAGCTCACGACACCTGAAATGGAAGAAAAAAACT
PR1409	GCACCAATTAATGCTCCGGTGCCCGTC
PR1410	GGTACTTCGGCGCGCCGCCACCATGGTGAGCAAGGGC
PR1411	GGTACTTCCTCGAGCTACTTGTACAGCTCGTCCATGCCGC
PR1446	CAACCAAAGAGATTCCTCATAAAAACCAAAGAGATTCCTCATAAAAACCAAAGAGATTC CTCATAAAC
PR1269	CGCGCCGGTTCAAAGTCCACA
PR1270	TATGTGGACTTTGAACCGG
PR1271	CGCGCCGGTTCAAAGTCCAGGTTCAAAGTCCACA
PR1272	TATGTGGACTTTGAACCTGGACTTTGAACCGG
PR1273	CGCGCCGGTTCAAAGTCCAGGTTCAAAGTCCAGGTTCAAAGTCCACA
PR1274	TATGTGGACTTTGAACCTGGACTTTGAACCTGGACTTTGAACCGG
PR1447	CCGGGTTTATGAGGAATCTCTTTGGTTTTTATGAGGAATCTCTTTGGTTTTTATGAGGAAT CTCTTTGGTTGGTAC
PR1796	CGCGCCCTACACAAAGCCCTCTGTGTAAGACA
PR1797	TATGTCTTACACAGAGGGCTTTGTGTAGGG
PR1798	CGCGCCCTACACAAAGCCCTCTGTGTAAGACTACACAAAGCCCTCTGTGTAAGACA
PR1799	TATGTCTTACACAGAGGGCTTTGTGTAGTCTTACACAGAGGGCTTTGTGTAGGG
PR1800	CGCGCCCTACACAAAGCCCTCTGTGTAAGACTACACAAAGCCCTCTGTGTAAGACTACAC AAAGCCCTCTGTGTAAGACA
PR1801	TATGTCTTACACAGAGGGCTTTGTGTAGTCTTACACAGAGGGCTTTGTGTAGTCTTACAC AGAGGGCTTTGTGTAGGG

PR1802	CGCGCCCTACACAAAGCCCTCTTTGTGAGACA
PR1803	TATGTCTCACAAAGAGGGCTTTGTGTAGGG
PR1804	CGCGCCCTACACAAAGCCCTCTTTGTGAGACTACACAAAGCCCTCTTTGTGAGACA
PR1805	TATGTCTCACAAAGAGGGCTTTGTGTAGTCTCACAAAGAGGGCTTTGTGTAGGG
PR1806	CGCGCCCTACACAAAGCCCTTACACAAAGAGACTACACAAAGCCCTTACACAAAGAGAC A
PR1807	TATGTCTCTTTGTGTAAGGGCTTTGTGTAGTCTCTTTGTGTAAGGGCTTTGTGTAGGG
PR1966	CGCGCCGGTTCAAAGTCCAGGTTCAAAGTCCAGGTTCAAAGTCCAGGTTCAAAGTCCAC A
PR1967	TATGTGGACTTTGAACCTGGACTTTGAACCTGGACTTTGAACCTGGACTTTGAACCGG
PR1979	GCACCATCCTAGATCTATGAGTCGAGGAGAGGTGCGCATGG
PR1980	GCACCATCCTCGGCCGAGATGGCGCCGGTCATGTCAGGCGGTGTGCTGGCA
PR2068	CGCGCCCTACACAAAGCCCTCTTTGTGAGACTACACAAAGCCCTCTTTGTGAGACTACAC AAAGCCCTCTTTGTGAGACA
PR2069	TATGTCTCACAAAGAGGGCTTTGTGTAGTCTCACAAAGAGGGCTTTGTGTAGTCTCACAA AGAGGGCTTTGTGTAGGG
PR2206	CGCGCCCGGGTTCAAAGTCCACA
PR2207	TATGTGGACTTTGAACCCGGG
PR2967	CCACTGACCGGTATGGTGCCCAAGAAGAAGAGGAAAG
PR2968	CCACTGGCTCTTCCGGAGTCCCCATCCTCGAGCAGC
PR3094	CGCGCCAGATCAAAGGGGGTACA
PR3095	TATGTACCCCCTTTGATCTGG
PR3096	CGCGCCAGATCAAAGGGGGTAAGATCAAAGGGGGTAAGATCAAAGGGGGTACA
PR3097	TATGTACCCCCTTTGATCTTACCCCCTTTGATCTTACCCCCTTTGATCTGG
PR3098	CGCGCCAGATCAAAGGGGGTAAGATCAAAGGGGGTAAGATCAAAGGGGGTA AGATCAAAGGGGGTAAGATCAAAGGGGGTAAGATCAAAGGGGGTACA
PR3099	TATGTACCCCCTTTGATCTTACCCCCTTTGATCTTACCCCCTTTGATCT TACCCCCTTTGATCTTACCCCCTTTGATCTTACCCCCTTTGATCTGG
PR3104	CGCGCCGGAGGAAAAACTGTTTCATACAGAAGGCGTCA
PR3105	TATGACGCCTTCTGTATGAAACAGTTTTTCCTCCGG
PR3106	CGCGCCGGAGGAAAAACTGTTTCATACAGAAGGCGTGGAGGAAAAACTGTTTCATACAG AAGGCGTCA
PR3107	TATGACGCCTTCTGTATGAAACAGTTTTTCCTCCACGCCTTCTGTATGAAACAGTTTTTCC TCCGG
PR2465	CGCGCCGGAGGAAAAACTGTTTCATACAGAAGGCGTGGAGGAAAAACTGTTTCATACAG AAGGCGTGGAGGAAAAACTGTTTCATACAGAAGGCGTCA
PR2466	TATGACGCCTTCTGTATGAAACAGTTTTTCCTCCACGCCTTCTGTATGAAACAGTTTTTCC TCCACGCCTTCTGTATGAAACAGTTTTTCCTCCGG
PR3217	CGCGCCGACCTTGAGTACGTGCGTCTCTGCACGTATGCA
PR3218	TATGCATACGTGCAGAGACGCACGTACTCAAGGTCGG
PR3219	CGCGCCGACCTTGAGTACGTGCGTCTCTGCACGTATGGACCTTGAGTACGTGCGTCTCTG CACGTATGCA
PR3220	TATGCATACGTGCAGAGACGCACGTACTCAAGGTCCATACGTGCAGAGACGCACGTACT CAAGGTCGG
PR3221	CGCGCCGACCTTGAGTACGTGCGTCTCTGCACGTATGGACCTTGAGTACGTGCGTCTCTG CACGTATGGACCTTGAGTACGTGCGTCTCTGCACGTATGCA
PR3222	TATGCATACGTGCAGAGACGCACGTACTCAAGGTCCATACGTGCAGAGACGCACGTACT CAAGGTCCATACGTGCAGAGACGCACGTACTCAAGGTCGG
PR0761	GCACCAACCGGTCGCCACCATGGTGCCCAAGAAG
PR0763	GCAGCTAAGCTTCTAGAGTCACTAGTTCAGTCCCCATCC
PR0726	CGTGTTTTTCTACAACTGGTTT
PR0727	AGAACTGGACGGGCTGC
PR0504	TATAGAATTCGCCACCATGGTGAGCAAGGGCGAGGAGGATAACAT
PR0550	TATATATCGGCCGCTACTTGTACAGCTCGTCCATGC
PR0534	CAATGCTAGCGCCTCAGACAGTGGTTCAAAG
PR0535	CAGCCACCACCTTCTGATAGG
BA1.68.5	CCTTCATATGTAGGCGTGTACGGTGGGA
BA1.68.7	CCAACCACTAGTGCGATCTGACGGTTCACT

gBlock042	ATGAGTCGAGGAGAGGTGCGCATGGCGAAGGCAGGACGAGAGGGACCACGGGACAGCG TGTGGCTGTCAGGAGAGGGACGGCGCGGCGGTCGCCGTGGAGGACAGCCGTCCGGGCTC GACCGAGACCGGCTCGAGGCCGCCACAGTAGTGCTGAAGCGTTGCGGTCCCATAGAGTT CACGCTCAGCGGAGTAGCAAAGGAGGTGGGGCTCTCCCGCGCAGCGTTAATCCAGCGCT TCACCAACCGCGATACACTGCTGGTGAGGATGGCCCTGGACGCCGTCTTCGGCGAGCTGC GCCACCCAGACCCGGACGCCGGACTCGACTGGCGAGAGGAACTGCGGGCCCTGGCCCGA GAGAACCGGGCACTGCTGGTGCGCCACCCTTGGTCTTCACGGCTGGTCGGCACCTACCTC AACATCGGACCACACTCGCTGGCCTTCTCTCGCGCGGTGCAGAACGTCGTGCGCCGCAGC GGACTGCCAGCACACCGCCTGACA

Table S4. Attached File, Related to Material and Methods. Transfection tables: DNA amounts and plasmid setup used for each experiment. Each Excel sheet is named with a Figure number and panel name and contains the experimental setup to produce the relative panel.

Supplemental Experimental Procedures

Minimal promoter design. In the prototypical core promoter the TATA box is the only AT-rich sequence embedded in a GC rich environment. Several works show the importance of the upstream (BRE^u) and downstream (BRE^d) sequence in modulating transcription initiation. It is well established from *in vitro* experiment that the BRE^u sequence mediates the interaction between the core promoter and the TFIIB core component of the initiation complex (Lagrange et al, 1998). In vitro transcription experiments in mammalian cell-extracts show that as a general trend a reduction in the GC content of the BRE^u reduce the basal level of transcription and the affinity for TFIIB (Wolner & Gralla, 2000).

Based on these observations the upstream sequence of our core promoter was derived from the TATA of E1B Adenovirus (Chen & Manley, 2003) while the rest of the sequence conforms to the classic consensus (Wolner & Gralla, 2000). This BRE^u harbors an imperfect consensus with intermediate GC content and near-background levels of TBP and TFIIB occupancy in vivo that can be increased by transcriptional activation. We call the resulting core promoter TATA Tight (TCTAGAGGGTATATAATGGGGGCCA, yellow shading representing the E1B-derived sequence and the cyan sequence being the consensus). We note that this exact sequence is not found in nature as verified by BLAST.

Response Elements design and promoter architecture. The sequence for the HNF1 response element (AGTTAATAATTTAAC) was derived from the published Positional Weight Matrix using the nucleotides with highest frequency for each position (Tronche et al, 1997a). Despite some differences in the gene activation profile between the two transcription factors (Senkel et al, 2005) the consensus sequence is known to bind both to HNF1A and HNF1B since the two TF share a highly conserved DNA binding domain (Wu et al, 2004).

Response elements in natural promoter often occur with periodic spacing related to DNA phasing (Larsson et al, 2007) and several works tried to test the relation between phasing and transcriptional response in small cis-regulatory modules (Huang et al, 2012). Different minimal promoter architectures were obtained by introducing a variable number of RE in direct tandem repeat or with an intervening 10 bp spacing. The spacer sequence (GCCGCTTAAA) was verified through TRANSFAC DB to confirm the absence of conserved transcription factor binding sites. Since the length of the HNF1 response element is 15 bp, this distance keeps the same DNA helical phasing between the centers of the response element but increase the distance potentially having an influence on the steric interactions.

The sequence for the HNF4A Response Element (GGTTCAAAGTCCA) was chosen over the classic Wild Type based on extensive measurement of DNA binding specificity by protein binding microarrays (Fang et al, 2012) in order to minimize the crosstalk with closely related Nuclear Receptors (RXRa and COUPTF2).

The SOX10 C-C' Response Element (CTACACAAAGCCCTCTGTGTAAGA) differs from the perfect consensus. It is based on the myelin Protein zero (P_0) promoter and is composed of two heptameric elements facing each other and separated by a 4bp spacing (Peirano & Wegner, 2000). The two sites have different affinities for the transcription factor high (C) and low (C') respectively. This arrangement favor dimeric binding improving the specificity for members of SOX group E (SOX8, SOX9 and SOX10) since group E is the only with a conserved dimerization domain (Kuhlbrodt et al, 1998). The SOX10 C-C Response Element (CTACACAAAGCCCTCTTTGTGAGA) is obtained by substituting the low affinity element with a second high affinity site. The resulting sequence was shown to bind SOX10 with higher affinity in vitro.

The sequence for the Hypoxya (HIF1A) Response Element (GACCTTGAGTACGTGCGTCTCTGCACGTATG) was selected based on the PWM derived by Chip-seq experiments (Schodel et al, 2011) and on previous observation suggesting that sequences flanking the minimal HIF1 consensus are important for efficient gene induction (Takagi et al, 1996).

The NFATC1 Response Element (GGAGGAAAAACTGTTTCATACAGAAGGCGT) is derived from the high affinity sequence in the IL-2 promoter (Fiering et al, 1990).

The sequence for the TCF/LEF Response Element (AGATCAAAGGGGGTA) was tested in human cell lines in (Buckley et al, 2015) and based on the previously published Top Flash reporter (Veeman et al, 2003).

Plasmid Construction. Plasmids were constructed using standard cloning techniques. All restriction enzymes used in this work were purchased from New England Biolabs (NEB). Phusion High-Fidelity DNA Polymerase (NEB) was used for fragment amplification. Single-strand oligonucleotides were synthesized by Microsynth or Sigma-Aldrich. Digestion products or PCR fragments were purified using GenElute Gel Extraction Kit or Gen Elute PCR Clean Up Kit (Sigma-Aldrich). Ligations were performed using T4 DNA Ligase (NEB) optimizing temperature, ligation time and molar ratio on a case by case basis. The ligation products were transformed into chemically competent *E.Coli* DH5α that were plated on LB Agar with appropriate antibiotics selection (Ampicillin, 100 µg/ml, Chloramphenicol, 25 µg/ml, Kanamycin, 50 µg/ml). The resulting clones where screened directly by colony-PCR whenever possible (Dream Taq Green PCR Master Mix, Thermo Scientific). We expanded single clones in LB Broth Miller Difco (BD) supplemented with the appropriate

antibiotics and purified their plasmid DNA using GenElute Plasmid Miniprep Kit (Sigma-Aldrich). All the resulting plasmids were verified by Microsynth using Sanger Sequencing. The DNA for mammalian transfection was obtained from 100 ml of liquid culture using the Invitrogen PureLink® HiPure Plasmid Maxiprep Kit (K2100-06). The recovered DNA was further purified using the Norgen Endotoxin Removal Kit Midi (Cat. # 52200) or Maxi (Cat.# 21900). A short cloning procedure for each construct used within this work is described in the Supplemental Information. The transcription factors cDNA used in this study where obtained from the I.M.A.G.E. Consortium library of Human cDNA or produced by RT-PCR in our laboratory (see construct pBA248 below). HNF1A (Clone IRATp970D08125D), HNF1B (clonbe IRATp970A0421D), SOX9 (clone IRATp970C0581D) and SOX10 (clone IRAUp969C0422D) were ordered from SourceBioscience as I.M.A.G.E clones. Primers are listed in Table S2. Specific cloning steps of the constructs employed in this study are as follows:

2x-sp HNF1A/B RE minTATA Cyan F4 (pBA001): pRheo-AmCyan-FF4 Backbone (Leisner et al, 2010) was amplified using primers PR0125 and PR0126 in order to remove the Rheo promoter region and adding AscI and SpeI restriction sites. The resulting product was gel purified, digested and ligated with the annealed oligos PR0121 and PR0122 in order to introduce a 2X Spaced HNF1 response elements flanked by a NdeI restriction site and a downstream minimal TATA Box. The resulting backbone has a modular promoter region that can easily be used to build families of transcriptional reporters or libraries. To obtain reporters with different transcription factors sensitivities pBA001 is digested with AscI and NdeI and ligated with different annealed oligos with matching overhangs. The HNF1 response element is designed according to the PWM described in (Tronche et al, 1997b)

4x-sp HNF1A/B RE minTATA Cyan-F4 (pBA002): PR0123 and PR0124

1x HNF1A/B RE minTATA Cyan-F4 (pBA004): Oligos BA1.68.1 and BA1.68.2

2x HNF1A/B RE minTATA Cyan-F4 (pBA067): Oligos PR0604 and PR0605

3x HNF1A/B RE minTATA Cyan-F4 (pBA068): Oligos PR0606 and PR0607

4x HNF1A/B RE minTATA Cyan-F4 (pBA005): Oligos BA1.68.3 and BA1.68.4

1x HNF1A/B RE CMV_{MIN} Cyan-F4- (pBA006): The CMV_{MIN} promoter was PCR amplified from pTRE-Tight-BI (Clontech Catalog # 631068) using BA1.68.5 and BA1.68.7 primers. The resulting fragment was digested with NdeI and SpeI and cloned in pBA004 linearized using the same restriction enzymes.

CMV Cyan-F4 (pBA008): pBA001 is digested using PciI and NheI to remove completely the promoter region. The CMV promoter is extracted from pAmCyan1-C1 Vector (Clontech #632441) using the same restriction enzymes and cloned in pBA001. The resulting backbone can be used as a strong positive control for response/transduction.

PIR 1x HNF1A/B RE minTATA Cyan F4 (pBA017): Upstream regulatory sequence can be introduced in all the original reporter backbone by digesting with PciI and AscI and ligating annealed oligos with matching overhangs. pBA004 is digested and ligated with annealed PR421 and PR422.

PIR 4x HNF1A/B RE minTATA Cyan F4 (pBA018): pBA005 is digested with PciI and AscI and ligated with PR421 and PR422.

PIR 1x HNF1A/B RE CMV_{MIN} Cyan-F4- (pBA019): pBA006 is digested with PciI and AscI and ligated with PR421 and PR422.

CMV Cyan-F4-PIT2 (pBA012): PIT2 (Pip-p65) was amplified from pMF208 ((Weber et al, 2002)) using PR0387 and PR0388 the resulting product was digested with BglII and HindIII, and cloned into pBA008 digested with the same enzymes to obtain a Cyan-Transactivator fusion protein.

CMV Cyan-F4-2A (pBA022): pBA008 was digested with BspeI and BglII and annealed oligos PR0431 and PR0432 harboring matching overhangs coding for the 2A Viral peptide in order to obtain a bicistronic expression unit.

CMV Cyan-F4-2A-PIT2 (pBA023): PIT2 was extracted from pBA012 with BglII and HindIII and subcolned into pBA022 using the same enzymes resulting in a bicistronic Cyan – Transactivator protein.

PIR 4x HNF1A/B RE minTATA Cyan-F4-2A-PIT2 (pBA028): The coding region (Cyan-F4-2A-PIT2) was extracted from pBA023 cutting with AgeI and HindIII and cloned in pBA018 using the same restriction enzymes.

Similar to pBA001 the resulting backbone can be used as a template for the creation of the different PIT2 feedback amplified transcriptional reporters using the same oligos discussed before. In particular in this study we build and use:

PIR RE 2x-sp HNF1A/B RE minTATA Cyan F4- 2A-PIT2 (pBA141): Oligos BA1.68.3 and BA1.68.4

PIR RE 2x HNF1A/B RE minTATA Cyan F4- 2A-PIT2 (pBA065): Oligos PR604 and PR605

PIR RE 3x HNF1A/B RE minTATA Cyan F4- 2A-PIT2 (pBA066): Oligos PR606 and PR607

PIR RE 4x-sp HNF1A/B RE minTATA Cyan F4- 2A-PIT2 (pBA328): PR0123 and PR0124

PIR RE 1x HNF1A/B RE minTATA Cyan F4- 2A-PIT2 (pBA027): The coding region (Cyan-F4-2A-PIT2) was extracted from pBA023 cutting with AgeI and HindIII and subcloned in pBA017 using the same restriction enzymes.

CMV iRFP (pCS12): Addgene plasmid 31857

pBA142 (HNF1B in pCMVSport6): I.M.A.G.E. Clone IRATp970D08125D

pEM002 (HNF1A in pCMVSport6): I.M.A.G.E. Clone IRATp970A0421D

pEM001 (pTRE-Bi mCherry-HNF1B): Extract HNF1B coding sequence from pBA142 using EcoRI and XbaI and ligate in pIM003 digested using the same restriction enzymes.

pTRE-Bi mCherry-HNF1A (pEM003): The pIM003 was digested with EcoRI,,the resulting overhang was blunted using NEB Quick Blunting Kit (# E1201S) and the resulting linearized backbone was cut with NotI. pEM002 was digested with SpeI, blunted as previously described, and digested again with NotI to extract the HNf1A coding sequence. The two resulting compatible fragments were ligated overnight at 16°C

1x HNF4A RE minTATA Cyan-F4 (pBA160): pBA001 is digested with AscI and NdeI and ligated with annealed oligos (PR1269-PR1270) harboring matching overhangs. The HNF4A specific response element is designed according to the PWM described in (Fang et al, 2012). In this study we similarly construct and use:

2x HNF4A RE minTATA Cyan-F4 (pBA161): Oligos PR1271-PR1272

3x HNF4A RE minTATA Cyan-F4 (pBA162): Oligos PR1273-PR1274

Pir 1x HNF4A RE minTATA Cyan-F4-2A-PIT2 (pBA163): A HNF1 Feedback Loop backbone (pBA141) was digested with AscI and NdeI and ligated with annealed oligos (PR1269-PR1270) harboring matching overhangs. In this study we similarly construct and use:

PIR 2x HNF4A RE minTATA Cyan-F4-2A-PIT2 (pBA163): Oligos PR1271-PR1272

PIR 3x HNF4A RE minTATA Cyan-F4-2A-PIT2 (pBA163): Oligos PR1273-PR1274

1x SOX9/10 C-C' RE minTATA Cyan-F4 (pBA342): pBA001 was digested with AscI and NdeI and ligated with annealed oligos (PR1796-PR1797) harboring matching overhangs. The SOX response element is designed according to (Peirano & Wegner, 2000). In this study we similarly construct and use:

2x SOX9/10 C-C' RE minTATA Cyan-F4 (pBA343): Oligos PR1798-PR1799

3x SOX9/10 C-C' RE minTATA Cyan-F4 (pBA344): Oligos PR1800-PR1801

1x SOX9/10 C-C RE minTATA Cyan-F4 (pBA345): Oligos PR1802-PR1803

2x SOX9/10 C-C RE minTATA Cyan-F4 (pBA346): Oligos PR1804-PR1805

2x SOX9/10 C-C_{INV} RE minTATA Cyan-F4 (pBA347): Oligos PR1806-PR1807

3x SOX9/10 C-C RE minTATA Cyan-F4 (pBA489): Oligos PR2068-PR2069

PIR 1x SOX9/10 C-C' RE minTATA Cyan-F4-2A-PIT2 (pBA367): A HNF1 Feedback Loop backbone (pBA141) was digested with AscI and NdeI and ligated with annealed oligos (PR1796-PR1797) harboring matching overhangs. In this study we similarly construct and use:

PIR 2x SOX9/10 C-C' RE minTATA Cyan-F4-2A-PIT2 (pBA368): Oligos PR1798-PR1799

PIR 3x SOX9/10 C-C' RE minTATA Cyan-F4-2A-PIT2 (pBA369): Oligos PR1800-PR1801

PIR 1x SOX9/10 C-C RE minTATA Cyan-F4-2A-PIT2 (pBA370): Oligos PR1802-PR1803

PIR 2x SOX9/10 C-C RE minTATA Cyan-F4-2A-PIT2 (pBA371): Oligos PR1804-PR1805

PIR 2x SOX9/10 C-C_{INV} RE minTATA Cyan-F4-2A-PIT2 (pBA372): Oligos PR1806-PR1807

PIR 3x SOX9/10 C-C RE minTATA Cyan-F4-2A-PIT2 (pBA477): Oligos PR2068-PR2069

pTRE Bidirectional mCherry-HNF4A (pBA266): pBA248 was digested with AgeI and PsPOMI and the resulting HNF4A coding region was cloned in the pIM003 backbone digested using the same restriction sites.

pTRE Bidirectional mCherry-SOX10 (pBA417): pBA402 was digested with XhoI, the resulting overhang was blunted using NEB Quick Blunting Kit (# E1201S). The linearized backbone was further digested with EcoRI, and the extracted TF band was cloned in pIM003 backbone in turn digested with NdeI, blunted as described above, and successively with EcoRI-HF.

pTRE Bidirectional mCherry-PIT2 (pBA427): PIT2 sequence was extracted from pMF206 by EcoRI and BamHI digestion. The sequence was cloned into pIM003 linearized using EcoRI and BamHI

pTRE Bidirectional mCherry-PITVP16 (pBA481): PITVP16 sequence was extracted from pMF156 by EcoRI and BamHI digestion. The sequence was cloned into pIM003 linearized using EcoRI and BamHI.

EF1A mCherry 3X FF3t 3XFF4t (pBA097): pKH026 was PCR amplified using the primers PR0700 and PR0702 adding the NotI and HindIII restriction sites and cloned in EF1a-ZsYellow-FF3x3-FF4x3 (Leisner et al, 2010).

EF1A mCherry 3X FF3t 3XFF4t (pBA098): pKH026 was PCR amplified using the primers PR0700 and PR0702 adding the NotI and HindIII restriction sites and cloned in EF1a-ZsYellow-FF5x3-FF6x3 (Leisner et al, 2010).

Cagop lox2272-loxP-mCherry$_{Inv}$- lox2272-loxP 3XFF4t (pBA221): The LoxP recombination sequence were amplified from pEL097(citation) with PR1012 and PR1013 adding AscI and KpnI restriction sites. mCherry was amplified from pKH026 using PR1410 and PR1411 introducing terminal XhoI and AscI restriction sites. pNL67 (citation) was digested with XhoI and KpnI. All the components were gel purified and a 3-Way Ligation was carried out overnight at 4°C.

EF1A lox2272-loxP-mCherry$_{Inv}$- lox2272-loxP 3XFF4t (pBA224): EF1A promoter was amplified from pKH026 adding using PR1402 and PR1409, the resulting product was digested with AseI and NheI. The promoter was cloned in the pBA221 backbone digested with the same restriction sites.

EF1A lox2272-mCherry- loxP 3XFF4t (pBA225): pBA225 was obtained starting from pBA224 by in vitro recombination using NEB Cre Recombinase (#M0298S), following the suggested protocol.

EF1A lox2272-loxP-mCherry$_{Inv}$- lox2272-loxP 3XFF6t (pBA235): pBA224 was digested with KpnI and XmaI. The resulting product was gel purified and ligated with the annealed oligos PR1446 and PR1447 harboring 3x FF6t flanked by matching overhangs.

EF1A lox2272-mCherry- loxP 3XFF6t (pBA237): pBA224 was digested with KpnI and XmaI. The resulting product was gel purified and ligated with the annealed oligos PR1446 and PR1447 harboring 3x FF6t flanked by matching overhangs.

PIR RE 2x HNF1A/B RE minTATA Cyan F4- 2A-PIT* (pBA435): gBlock042 encoding a mutated version of PIT2 was amplified using PR1979 and PR1980. The product was digested with BglII and EagI and cloned in pBA065 digested with the same restriction enzymes.

pCMV – HNF4A (pBA248): HNF4A cDNA was obtained by extracting the mRNA from HuH-7 cell line using the mirVana miRNA Isolation Kit (Life Techonologies) according to the protocol for Total RNA isolation. The resulting pool was retro-transcribed with the Maxima H Minus First Strand cDNA Synthesis Kit (Thermo Scientific) using the specific primers pair described in (Takagi et al, 2010) and according to the suggested RT conditions. The resulting double stranded DNA was amplified with PR1516 and PR1518 and cloned in pBA008 digested with the same pair of enzymes to produce a constitutive ectopic version of HNF4A

PIR RE 1x HNF1A/B RE minTATA Cyan F4- 2A-PIT* (pBA436): gBlock042 encoding a mutated version of PIT2 was amplified using PR1979 and PR1980. The product was digested with BglII and EagI and cloned in pBA027 digested with the same restriction enzymes.

PIR RE 3x HNF1A/B RE minTATA Cyan F4- 2A-PIT* (pBA437): gBlock042 encoding a mutated version of PIT2 was amplified using PR1979 and PR1980. The product was digested with BglII and EagI and cloned in pBA066 digested with the same restriction enzymes.

PIR RE 1x HNF4A RE minTATA Cyan F4- 2A-PIT* (pBA478): pBA435 was digested with AscI and NdeI and ligated with annealed oligos (PR1269-PR1270) harboring matching overhangs. Using the same strategy we construct also:

PIR RE 3x HNF4A RE minTATA Cyan F4- 2A-PIT* (pBA479): Oligos PR1273-PR1274

PIR RE 2x HNF4A RE minTATA Cyan F4- 2A-PIT* (pBA507): Oligos PR1271-PR1272

PIR RE 4x HNF4A RE minTATA Cyan F4- 2A-PIT* (pBA508): Oligos PR1966-PR1967

PIR RE 1X+2sp HNF4A RE minTATA Cyan F4- 2A-PIT* (pBA509): Oligos PR2206-PR2207

Pir 3x SOX9/10 C-C RE minTATA Cyan-F4-2A-PIT* (pBA480): pBA435 was digested with AscI and NdeI and ligated with annealed oligos (Oligos PR2068-PR2069) harboring matching overhangs. Using the same strategy we construct also:

PIR RE 1x SOX9/10 C-C' RE minTATA Cyan F4- 2A-PIT* (pBA512): Oligos PR1796-PR1797

PIR RE 1x SOX9/10 C-C RE minTATA Cyan F4- 2A-PIT* (pBA513): Oligos PR1802-PR1803

PIR RE 2x SOX9/10 C-C' RE minTATA Cyan F4- 2A-PIT* (pBA514): Oligos PR1798-PR1799

PIR RE 2x SOX9/10 C-C RE minTATA Cyan F4- 2A-PIT* (pBA515): Oligos PR1804-PR1805

PIR RE 3x SOX9/10 C-C' RE minTATA Cyan F4- 2A-PIT* (pBA516): Oligos PR1800-PR1801

PIR 1x HNF1A/B RE CMV_{MIN} Cyan-F4-2A-PIT* (pBA492): Cyan-2A-PIT* is extracted from pBA435 by digestion with AgeI and HindIII. The sequence is cloned in pBA019 backbone digested with the same enzymes

PIR 2x HNF1A/B RE CMV_{MIN} Cyan-F4-2A-PIT* (pBH289): pBA492 is digested with AscI and NdeI and ligated with annealed oligos PR0604 – PR0605

PIR 3x HNF1A/B RE CMV_{MIN} Cyan-F4-2A-PIT* (pBH290): pBA492 is digested with AscI and NdeI and ligated with annealed oligos PR0606 – PR0607

PIR 1x HNF1A/B RE CMV_{MIN} Cyan-F4-2A-PIT2 (pBA493): The Cyan-2A-PIT2 is extracted from pBA165 by digestion with AgeI and HindIII. The sequence is cloned in pBA019 backbone digested with the same enzymes.

PIR 2x HNF1A/B RE CMV_{MIN} Cyan-F4-2A-PIT2 (pBH291): pBA493 is digested with AscI and NdeI and ligated with annealed oligos PR0604 – PR0605

PIR 3x HNF1A/B RE CMV_{MIN} Cyan-F4-2A-PIT2 (pBH292): pBA493 is digested with AscI and NdeI and ligated with annealed oligos PR0606 – PR0607

CMV Cyan-F4-2A-PIT2 (pBA528): The Cyan-2A-PIT2 is extracted from pBA435 by digestion with AgeI and HindIII. The sequence is cloned in pBA019 backbone digested with the same enzymes.

pEL0172 Pir 30bp Spacer mCitrine (pEL0172): As described (Prochazka et al, 2014).

Ef1A iCRE (pNL108): As described (Lapique & Benenson, 2014).

Ef1α-mCherry (pKH026): mCherry was PCR amplified from Addgene plasmid 30125 (pKH015) using primers PR0504 and PR0550 and cloned into Addgene plasmid 11154 (pKH013) after digestion with EcoRI and EagI

pTRE Bidirectional mCherry-pA (pIM003): mCherry was amplified from pKH0026 with primers PR0534 and PR0535, digested with KpnI and MluI and cloned in pTRE-Bi (Clontech# 631068)

PIR 3X HNF1A Cre-2A-PIT2 (pBA703): PCR amplify pNL108 with PR2967-PR2968 digest AgeI-BspQI and clone in pBA066 digested with the same enzymes.

PIR 3X C-C Cre-2A-PIT2 (pBA707): PCR amplify pNL108 with PR2967-PR2968 digest AgeI-BspQI and clone in pBA477 digested with the same enzymes.

PIR RE 1x TCF/LEF RE minTATA Cyan F4- 2A-PIT* (pBA790): pBA435 was digested with AscI and NdeI and ligated with annealed oligos (PR3094-PR3095) harboring matching overhangs. Using the same strategy we construct also:

PIR RE 3x TCF/LEF RE minTATA Cyan F4- 2A-PIT* (pBA791): Oligos PR3096-PR3097

PIR RE 6x TCF/LEF RE minTATA Cyan F4- 2A-PIT* (pBA791B): Oligos PR3098-PR3099

PIR RE 3x NFATC1 RE minTATA Cyan F4- 2A-PIT* (pBA612): pBA435 was digested with AscI and NdeI and ligated with annealed oligos (PR2465-PR2466) harboring matching overhangs. Using the same strategy we construct also:

PIR RE 1x NFATC1 RE minTATA Cyan F4- 2A-PIT* (pBA794): Oligos PR3104-PR3105

PIR RE 2x NFATC1 RE minTATA Cyan F4- 2A-PIT* (pBA795): Oligos PR3106-PR3107

PIR RE 1x HIF1 RE minTATA Cyan F4- 2A-PIT* (pBA826): pBA435 was digested with AscI and NdeI and ligated with annealed oligos (PR3217-PR3218) harboring matching overhangs. Using the same strategy we construct also:

PIR RE 2x HIF1 RE minTATA Cyan F4- 2A-PIT* (pBA827): Oligos PR3219-PR3220

PIR RE 3x HIF1 RE minTATA Cyan F4- 2A-PIT* (pBA828): Oligos PR3221-PR3222

PIR 1x TCF/LEF RE minTATA Cyan-F4-2A-PIT2 (pBA802): A HNF1 Feedback Loop backbone (pBA141) was digested with AscI and NdeI and ligated with annealed oligos (PR3094-PR3095) harboring matching overhangs. In this study we similarly construct and use:

PIR RE 3x TCF/LEF RE minTATA Cyan F4- 2A-PIT2 (pBA802): Oligos PR3096-PR3097

PIR RE 6x TCF/LEF RE minTATA Cyan F4- 2A-PIT2 (pBA803): Oligos PR3098-PR3099

PIR RE 3x NFATC1 RE minTATA Cyan F4- 2A-PIT2 (pBA612): A HNF1 Feedback Loop backbone (pBA141) was digested with AscI and NdeI and ligated with annealed oligos (PR2465-PR2466) harboring matching overhangs. Using the same strategy we construct also:

PIR RE 1x NFATC1 RE minTATA Cyan F4- 2A-PIT2 (pBA807): Oligos PR3104-PR3105

PIR RE 2x NFATC1 RE minTATA Cyan F4- 2A-PIT2 (pBA808): Oligos PR3106-PR3107

PIR RE 1x HIF1A RE minTATA Cyan F4- 2A-PIT2 (pBA820): A HNF1 Feedback Loop backbone (pBA141) was digested with AscI and NdeI and ligated with annealed oligos (PR3217-PR3218) harboring matching overhangs. Using the same strategy we construct also:

PIR RE 2x HIF1A RE minTATA Cyan F4- 2A-PIT2 (pBA821): Oligos PR3219-PR3220

PIR RE 3x HIF1A RE minTATA Cyan F4- 2A-PIT2 (pBA822): Oligos PR3221-PR3222

pTRE Bidirectional mCherry- CA-NFATC1 (pBA888B): CA-NFATC1 coding sequence was PCR amplified from Addegene Plasmid #11102 (CA-NFAT2) with primers PR3329-PR3330 digested with AgeI and PsPOMI and cloned in the pIM003 backbone digested using the same restriction sites.

Representative minimal promoters. We show here as an example the 3X sensors promoters. The PIR (PIT Response Element) is in red, the different transcription factor specific response elements are depicted in blue, the sequence of our minimal TATA is in green and the starting codon of the coding sequence (ATG) is in bold. The distance is counted starting from the center of the PIR (G in bold red) to the base preceding the TATAAT consensus (G in bold green).

PIT R.E. TF RE min minTATA **Start Codon**

3X HNF1A:

GAAATAGCGCTGTACAGCGTATGGGAATCTCTT**G**TACGGTGTACGAGTATCTTCCCGTACACCGTACGGCGCGCCAGTTAA
TAATTAACTAGTTAATAATTAACTAGTTAATAATTAACTCATATGCTCTAGAGG**G**TATATAATGGGGGCCACTAGTCTACT
ACCAGAGCTCATCGCTAGCGCTACCGGTCGCCACC**ATG**

3X HNF4A:

GAAATAGCGCTGTACAGCGTATGGGAATCTCTT**G**TACGGTGTACGAGTATCTTCCCGTACACCGTACGGCGCGCCGGTTCA
AAGTCCAGGTTCAAAGTCCAGGTTCAAAGTCCACATATGCTCTAGAGG**G**TATATAATGGGGGCCACTAGTCTACTACCAGA
GCTCATCGCTAGCGCTACCGGTCGCCACC**ATG**

3X C-C SOX10:

GAAATAGCGCTGTACAGCGTATGGGAATCTCTT**G**TACGGTGTACGAGTATCTTCCCGTACACCGTACGGCGCGCCCTACAC
AAAGCCCTCTTTGTGAGACTACACAAAGCCCTCTTTGTGAGACTACACAAAGCCCTCTTTGTGAGACATATGCTCTAGAGG
GTATATAATGGGGGCCACTAGTCTACTACCAGAGCTCATCGCTAGCGCTACCGGTCGCCACC**ATG**

3X HIF1A:

GAAATAGCGCTGTACAGCGTATGGGAATCTCTT**G**TACGGTGTACGAGTATCTTCCCGTACACCGTACGGCGCGCCGACCTT
GAGTACGTGCGTCTCTGCACGTATGGACCTTGAGTACGTGCGTCTCTGCACGTATGGACCTTGAGTACGTGCGTCTCTGCA
CGTATGCATATGCTCTAGAGGG**T**ATATAATGGGGGCCACTAGTCTACTACCAGAGCTCATCGCTAGCGCTACCGGTCGCCA
CC**ATG**

3X TCF/LEF:
GAAATAGCGCTGTACAGCGTATGGGAATCTCTT**G**TACGGTGTACGAGTATCTTCCCGTACACCGTACGGCGCGCCAGATCA
AAGGGGGTAAGATCAAAGGGGGTAAGATCAAAGGGGGTACATATGCTCTAGAGG**G**TATATAATGGGGGCCACTAGTCTACT
ACCAGAGCTCATCGCTAGCGCTACCGGTCGCCACC**ATG**

3X NFATC1:
GAAATAGCGCTGTACAGCGTATGGGAATCTCTT**G**TACGGTGTACGAGTATCTTCCCGTACACCGTACGGCGCGCCGGAGGA
AAAACTGTTTCATACAGAAGGCGTGGAGGAAAAACTGTTTCATACAGAAGGCGTGGAGGAAAAACTGTTTCATACAGAAGG
CGTCATATGCTCTAGAGG**G**TATATAATGGGGGCCACTAGTCTACTACCAGAGCTCATCGCTAGCGCTACCGGTCGCCACC**A**
TG

Cell culture and transfection procedure. The experiments in this work are performed on five different cell lines: HEK293 Tet-On Advanced, HEK293, HuH-7, HeLa and HCT-116. HEK293 Tet-On Advanced cell lines were originally purchased from Clontech (Cat # 630931) and HEK293 (293-H) cells were purchased from Invitrogen (Cat # 11631-017).

HCT-116 were purchased from the Deutsche Sammlung von Mikroorganismen und Zellkulturen (DSMZ) (cat. no. ACC581). Both HEK293 lines were cultured at 37 ºC, 5% CO_2 in RPMI-1640 medium (Gibco, Life Technologies; Cat # A10491-01), supplemented with 10% FBS (Sigma-Aldrich; Cat # F9665). Splitting was performed every 3-4 days using 0.25% Trypsin- EDTA (Gibco, Life technologies; Cat # 25200-072). HuH-7 cells were purchased from the Health Science Research Resources bank of the Japan Health Sciences Foundation (Cat-# JCRB0403, Lot-# 07152011) and cultured at 37 °C, 5% CO_2 in DMEM, low glucose, GlutaMAX (Life technologies, Cat #21885-025), supplemented with 10% FBS (Sigma-Aldrich, Cat #F9665 or Life technologies, Cat #10270106). HeLa cells were purchased from ATCC (Cat # CCL-2, Lot: 58930571) and cultured at 37°C, 5% CO_2 in DMEM, high glucose (Life technologies, Cat #41966), supplemented with 10% FBS (Sigma-Aldrich, Cat #F9665 or Life Technologies, Cat #10270106). All the media are supplemented with 1% Penicillin/Streptogamine Solution (Sigma-Aldrich, Cat #P4333). Cultures were propagated for at most two months before being replaced by fresh cell stock.

Transfections. All transfections were performed using Lipofectamine 2000 Transfection Reagent (Life Technologies) according to the suggested guidelines. All transfections used for data binning and fitting were performed in uncoated 6-well plates (Thermo Scientific Nunc) in order to collect a large number of single cell measurements. The cells were seeded 24 h before transfection at a density per well of 3.5 x 10^5 for HEK293 Tet-On and HEK293, 3x 10^5 for HeLa and 2.5x 10^5 for HuH-7 in order to have an 80-90% confluence at the time of transfection. The plasmids for each sample were mixed according to **Table S4** (see different tabs that refer to individual panels) and diluted into 250 μl of Opti-MEM I Reduced Serum (Gibco, Life technologies Cat # 31985-962). Lipofectamine 2000 was diluted in 250 μl Opti-MEM I per sample to a final amount of 2.5:1 ml Reagent/mg DNA ratio. After an incubation of 5 minutes the diluted Lipofectamine was added to the diluted DNA sample. The resulting mixture was briefly mixed by gentle vortexing and incubated 20 minutes at room temperature before being added to the cells. When required Doxycycline hyclate (Fluka, Cat # 44577) was added right after transfection starting from a 1000x stock to a 1000 ng/mL final concentration.

Microscopy. Microscopy images were taken 48 h after transfection. We used the Nikon Eclipse Ti microscope equipped with a mechanized stage and temperature control chamber held at 37 °C during the image acquisition. The excitation light was generated by a Nikon IntensiLight C-HGFI mercury lamp and filtered through a set of optimized Semrock filter cubes. The resulting images were collected by an Hammamatsu, ORCA R2 camera using a 10X objective. Each Semrock cube is assembled from an excitation filter, a dichroic mirror and an emission filter. In order to minimize the crosstalk between the different fluorescent proteins we used the following setup: **amCyan:** CFP HC (HC 438/24, BS 458, HC 483/32), **mCitrine**: YFP HC (HC 500/24, BS 520, HC 542/27), **mCherry:** TxRed HC (HC 624/40, BS 593, HC 562/40), **iRFP:** Cy5.5-A (HC 655/40, BS 685, HC 716/40). The images shown in Figure 6 were acquired with an exposure of 200 ms for AmCyan and 2 s for iRFP given the low sensitivity of CMOS sensors for the low energy part of the spectrum. The images in Figure 7 are recorded using an exposure of 200 ms for mCitrine, 800 ms for mCherry and keep the previous settings for AmCyan and iRFP. The acquired images were processed by ImageJ software performing uniform contrast-enhancement to improve visualization. All the images in each panel were treated with the same parameters.

Conversion factor between high and low PMT voltages for output measurements. To extend the measurement dynamic range for FACS measurements and cover with reasonable sensitivity values spanning several order of magnitudes, from the low expression levels of the uninduced open loop to the induced feedback loop response, we used two different PMT settings for Amcyan: 400V for the open loop measurements and 250V for the feedback loop measurements. To establish a conversion factor we measured the SPHERO RainBow Calibration particles at two different PMT and calculated the intensity ratio for each peak (**Figure S2A**). Since the particles are very uniform this method is extremely accurate. However, the beads emission in the Cyan channel is low compared to the levels reached by some of fluorescent constructs. Furthermore the amplification factor could be sensitive to the difference in the specific emission spectrum between the beads and AmCyan.

To validate the method we measured several samples containing AmCyan and iRFP at both PMTs for Cyan while keeping the iRFP PMT voltage constant between the two measurements. In this way the iRFP value can be used as a reference to relate two separate measurements. In particular the iRFP-Cyan data sets obtained in this way from both measurements were binned by similar iRFP values and a conversion factor for each pair was calculated by dividing the corresponding mean Cyan measured at PMT 400 by the one measured at PMT 250. All the generated data points were used to calculate a linear regression between the "conversion factors" and the iRFP levels (**Figure S2B**). The resulting linear fitting has a slight positive slope for increasing levels of cyan but can be approximated by a constant for an extended dynamic range. Ultimately, a constant factor of 28 was used for simplicity, since the exact value has very little effect on our data analysis.

Synergy Measurements Setup. In order to balance the DNA employed in the transfection, equalize transcriptional and translational load on cells and have comparable levels of mCherry when withholding the TF or the AA plasmids in Figure 3 experiments, we substitute it with an analogous inducible plasmid coding for mCherry and a balancing factor that does not trigger a response. This setup creates very similar experimental condition among the different states. To confirm that

the expression of balancing factors does not affect the observed synergy, we conducted a control experiment in which the transfection is balanced by plasmids expressing exclusively mCherry. We call this second configuration Unbalanced (**Figure S3F**). The synergistic behavior is conserved (**Figure S3G** left), and the measured synergy scores are not significantly affected by the absence of the balancing factor (**Figure S3G** right). To confirm that the synergy does not arise from interaction of the mutant PIT* protein with regulators, we remove PIT2* from the highest-synergy 3x HNF1A/B composite promoter so that it expresses the Cyan fluorescent reporter exclusively. The removal of PIT* does not result in a significant change in the observed synergy score (**Figure S3H**).

Distance definition in synergy measurements. All base pairs distances (bp) are calculated by counting from the center of the amplifier activator (AA) response element to the bp preceeding the TATA consensus sequence.

Synergy Score Calculation. Synergy is defined as the deviation from additive linear response and calculated as the ratio between the expression in the presence of both TF and AA, divided by the sum of expression with TF only and AA only. To yield more consistent results all the measurements in **Figure 3** are carried out at the same settings used for the feedback loop (PMT 250). Given the low expression level for TF only induction, the signal in these conditions is barely above background, reducing our ability to accurately discriminate differences between response element variants. To increase the precision of the calculation we use TF induction values derived from the measurements in **Figures 1 B-D** where we use high PMT and measure a large number of events. These measurements are then corrected for the factor of 5 introduced by the 2A element in the constructs used for synergy characterization (**Figure S3B**).

Forward engineered sensors measurements: HIF1A is induced by adding 250 μM of $COCl_2$ (Sigma C8661) 24h after transfection. (Li et al, 2006) TCF/LEF response is induced by adding 50 mM LiCl (Sigma 203637) 24h after transfection.(Li et al, 2006) NFATC1 activation is obtained through the ectopic expression of a NFATC1 calcium sensitive variant (pBA888B) successively induced by adding 10 ng/ml of PMA (Sigma P1585) and 0.5 mM of Ionomycin (Tocris 2092) 24h after transfection.(Boss et al, 1996) The cells were harvested and measured 48h after transfection resulting in a 24h stimulation time for all the chemical inducers.

AND gate measurements. The plasmid composition for the AND-gate characterization in Figure 6 are in **Table S4**. We note that balancing factors were used, similar to the procedure employed in synergy characterization.

Flow Cytometry. The cells were prepared for FACS analysis 48 h after transfection by removing the medium and incubating the cells with 300 ml phenol-red free Trypsin (0.5% Trypsin-EDTA (Gibco, Life Technologies, cat # 15400-054) at 37°C for 3 minutes (HEK293, HEK293 Tet-On) or 5-6 minutes (HuH-7 and HeLa). After incubation, the Trypsin concentration was diluted 1:2 with PBS (Gibco, Life Technologies cat # 10010-56) and the suspended cells were transferred to FACS tubes (Life Systems Design, Cat # 02-1412-000) and kept on ice. To avoid potential cell damage the samples were prepared in successive batches so that no single sample was kept on ice for more than 1 h. The prepared samples were measured using a BD LSR Fortessa II Cell Analyzer with a combination of excitation and emission that minimizes the crosstalk between different fluorescent reporters. AmCyan was measured with a 445 nm laser and a 473/10 nm emission filter, mCherry with a 561 nm excitation laser coupled to a 600 nm longpass filter and 610/20 emission filter, mCitrine with 488 nm laser, 505 nm longpass filter and 542/27 nm emission filter and iRFP using a 640 nm excitation laser and 710/50 emission filter. The iRFP transfection control was measured at PMT voltage of 300 in all the experiments, representing a constant baseline. Other PMT voltages were chosen to take the full advantage of the dynamic range, but were kept consistent in experiments that are directly compared. In particular, mCherry was measured using a PMT voltage of 300V in the TF induction experiments and 350 V when used as a target for downstream knockdown, but the two dataset are never compared. mCitrine is measured at 250 V. In order to extend the dynamic range, AmCyan is measured at 400 V in experiments with open loop sensor and at 250 V in experiments with feedback-amplified sensors, and at 300 V when the feedback loop is used to drive downstream repression. Several of the samples have been measured at different Cyan PMT voltages to build a conversion function and allow samples comparison across different PMT Values. SPHERO RainBow Calibration particles (Cat # 559123, BD) and Align Flow Cytometry beads (Cat # A16500, Life Technologies) were used to ensure constant device performance and to qualitatively validate the PMT conversion factors obtained for AmCyan.

Data Analysis. General flow cytometry data analysis for bar charts was performed using FlowJo software. In this work we use three different fluorescent units: absolute, relative and normalized. Absolute values (**abs. u.**) are the direct numerical values measured by the instrument; when feedback-amplified sensors are shown, these values are multiplied by the factor 28 to be comparable to open-loop sensors. These units are typically used to present binned data.

Relative expression units (**rel. u.**) are calculated as follows. (i) Live cells are gated based on their forward and side-scatter readouts. (ii) Within this gate, cells positive in a given fluorophore are gated based on a negative control such that 99.9% of cells in this single-color control sample fall outside of the selected gate. (iii) For each positive cell population in a

given channel, the mean value of the fluorescent intensity is calculated and multiplied by the frequency of the positive cells. This value is used as a measure for the total reporter signal in a sample and can be defined as Total Intensity (TI). The total intensity of a given output is normalized by the frequency of iRFP-positive cells (constitutive transfection control) to account for day-to-day variations in transfection efficiency or cell state. The procedure can be summarized in the following formula: Reporter intensity in rel. u. = [mean(Reporter in Reporter+ cells) * Frequency (Reporter+ cells)] / frequency (Transfection Marker+ cells). Relative units are used when we directly compare expression levels between different cell lines, since constitutive promoters of transfection control have very different strength in different cell lines and the use of normalized units (below) is inappropriate.

Normalized units (**norm. u**) are obtained by dividing the total intensity of the output of interest (as defined above) by the total intensity of the iRFP transfection control.
The relative formula is therefore: Reporter intensity in norm. u. = [mean(Reporter in Reporter+ cells) * Frequency (Reporter+ cells)] / [mean (Transfection Marker in Transfection Marker+ cells) * Frequency (Transfection Marker+ cells)]. Normalized units are a more robust indicator when the comparison is done between measurements taken from the same cell line.

The provided flow cytometry plot data are created through the FlowJo Layout editor and gated to show the same number of gated live cells (190000). The shown plots are selected as representative samples out of a biological triplicate.

Fine binning for the fitting. The flow cytometry data from a biological triplicate measurement containing in total 6-8 million cells for HEK293 Tet-On and 2-3 million cells with HuH-7, was exported without gating into csv format while pooling the triplicate data. The gating was performed in Matlab by a conservative oval gate on forward-side scatter plot to exclude dead cells and debris. All cells whose Cyan levels fell within a given bin were collected together and their value averaged. The bins were spaced at equal 1000 instrument units apart (with the entire range between -200 to 250000 units). Fitting was performed without weighting.

Modeling of open-loop binned data. The model of open loop induction with two genes reflecting the assay in HEK293 Tet-On cell was created using a system of differential equations. We model TF binding as a second-order process, resulting in an activation function with a Hill coefficient of 1, due to the lack of data that suggest otherwise. The explanation of the different terms is as follows:

$[HNF]$	Concentration of free HNF TF in a cell
$[G_{HNF}]$	Copy number of HNF-encoding gene in a cell
$[G_{Cyan}]$	Concentration of unbound sensor gene in a cell
$[G_{Cyan}::HNF]$	Concentration of the sensor gene bound to HNF factor in a cell
$[G_{Cyan}^{(0)}]$	Initial copy number of sensor gene in a cell
$[Cyan]$	Concentration of sensor output, AmCyan
$k_{syn}^{(1)}$	Lumped expression rate of HNF (DNAè Protein)
$k_{syn}^{(2)}$	Lumped expression rate of Cyan from TF-bound DNA complex (DNAè Protein)
k_{ON}^{HNF}	Association rate constant of HNF to its sensor
k_{OFF}^{HNF}	Dissociation rate of HNF from the bound complex
k_{DEG}^{HNF}	HNF degradation rate constant
k_{DEG}^{Cyan}	Cyan degradation rate constant

The mass-balance of the HNF transcription factor, expressed from the HNF-encoding gene G_{HNF}:

$$\frac{d[HNF]}{dt} = k_{syn}^{(1)}[G_{HNF}] - k_{ON}^{HNF}[G_{Cyan}][HNF] + k_{OFF}^{HNF}[G_{Cyan}::HNF] - k_{DEG}^{HNF}[HNF] \quad \text{(S.1)}$$

The mass-balance of HNF-bound sensor:

$$\frac{d[G_{Cyan}::HNF]}{dt} = k_{ON}^{HNF}[G_{Cyan}][HNF] - k_{OFF}^{HNF}[G_{Cyan}::HNF] \quad \text{(S.2)}$$

Mass-balance of Cyan:

$$\frac{d[Cyan]}{dt} = k_{syn}^{(2)}\left[G_{Cyan}::HNF\right] - k_{DEG}^{Cyan}[Cyan] \quad \text{(S.3)}$$

Mass-balance of bound and unbound sensor species:

$$[G_{Cyan}] = [G_{Cyan}^{(0)}] - \left[G_{Cyan}::HNF\right] \quad \text{(S.4)}$$

In the steady state, the analytical solution (Mathematica®) is as follows

$$[HNF] = k_{syn}^{(1)}\frac{G_{HNF}}{k_{DEG}^{HNF}} \quad \text{(S.5)}$$

$$[Cyan] = \frac{k_{syn}^{(2)}k_{ON}^{HNF}k_{syn}^{(1)}[G_{Cyan}^{(0)}][G_{HNF}]}{k_{DEG}^{Cyan}\left(k_{DEG}^{HNF}k_{OFF}^{HNF} + k_{ON}^{HNF}k_{syn}^{(1)}[G_{HNF}]\right)} \quad \text{(S.6)}$$

$$\left[G_{Cyan}::HNF\right] = \frac{k_{ON}^{HNF}k_{syn}^{(1)}[G_{Cyan}^{(0)}][G_{HNF}]}{k_{DEG}^{HNF}k_{OFF}^{HNF} + k_{ON}^{HNF}k_{syn}^{(1)}[G_{HNF}]} \quad \text{(S.7)}$$

We assume that in a co-transfection experiment,

$$[G_{Cyan}^{(0)}] = [G_{HNF}] = G$$

and then

$$[Cyan] = \frac{k_{syn}^{(2)}k_{ON}^{HNF}k_{syn}^{(1)}G^2}{k_{DEG}^{Cyan}\left(k_{DEG}^{HNF}k_{OFF}^{HNF} + k_{ON}^{HNF}k_{syn}^{(1)}G\right)} \quad \text{(S.8)}$$

This functional form can be fitted to the data obtained in measurements. The actual form used for fitting is

$$[AmCyan] = \frac{[mCherry]^2}{b_1 + b_2[mCherry]} + b_3 \quad \text{(S.9)}$$

Where

$$[mCherry] = \alpha[G]$$

(The linear relationship between the gene copy number and fluorescence was established in earlier work (Bleris et al, 2011))

Modeling of synergistic feedback amplification and simulations

The model was built in SimBiology Matlab toolbox (**Figure S4E**). In this model regulator binding is modeled as a second-order process, resulting in an activation function with a Hill coefficient of 1, due to the lack of data that suggest otherwise. The concentration is measured in "molecules", which means "molecules per mammalian cell" such that 1 "molecule" = 10^{-12} M (assuming cell volume of 1660 μm^3). The main processes and parameters are summarized below:

1. Expression of mCherry and ectopic TF from a DNA cassette. The cassette copy number is set to 10 to represent a mean copy number in a transent transfection. The processes are modeled as separate transcription and translation, with both mRNA and protein degraded in first-order processes. Transcription rate is 0.003 1/s and translation rate is 0.008 1/s. RNA degradation rate is $6*10^{-5}$ 1/s corresponding to half-life about about 3 hours, and protein degradation rate is $8.02*10^{-6}$ 1/s

for mCherry, corresponding to half-life of 24 hours (stable protein); and $1.6*10^{-5}$ 1/s for the TF, corresponding to half life of 12 hours.

2. Binding of activators to sensor DNA. Sensor DNA exists in four configurations: naked DNA; DNA complexed to a transcriptional input (DNA::TF); DNA complexed to an amplifier activator (DNA::AA) and DNA complexed to both (DNA::TF::AA). Spieces can interconvert through binding and unbinding of proteins. Unbinding of all proteins has a rate constant of 0.01 1/sec. Binding of proteins is as follows: TF binding rate constant ranges between 10^{-8} ... 10^{-5} $s^{-1}molecule^{-1}$. Binding rate constant of AA: 10^{-8} ... 10^{-5} $s^{-1}molecule^{-1}$. To avoid accumulation of bound species, they are also converting back to naked DNA with the rate that equals the general protein degradation rate of $1.6*10^{-5}$ 1/s.

3. Expression of output and amplifier activator (in the case of feedback). The three bound complexes can express RNA coding for an output and an amplifier activator. The expression rate from DNA::TF complex is set at $6*10^{-5}$ 1/s and from a DNA:TF::AA complex at 0.003 1/s (50 times higher). The expression from DNA::AA complex is set either at 0.003 1/s for lack of synergy, or at a lower number, corresponding to synergy factor. In most simulations it is set at $6*10^{-5}$ 1/s. There is a splicing step to desicribe the splicing of miR-FF4 (rate of 0.01 1/s) and the resulting mRNA is translated into AmCyan with the rate of 0.008 1/s and, in the case of positive feedback, also to AA with the same rate. To model the lack of feedback, this reaction rate is set to zero.

Figure 4E, Figure S4F: The binding rate constants of activators (TF and AA) were scanned in 10-fold increases from 10^{-8} to 10^{-5} $s^{-1}molecule^{-1}$. For each assignment of the binding rate constants, the expression rate of the TF was varied as indicated on the X axis. For the open-loop output simulation, the translation of AA was set to zero. For closed-loop, it was set to 0.008 1/s. For feedback without synergy, the expression rates for different complexes were as follows: DNA::TF: $6*10^{-5}$ 1/s; DNA::AA: 0.003 1/s; DNA::TF::AA: 0.003 1/s. For a feedback with synergy, as follows: DNA::TF: $6*10^{-5}$ 1/s; DNA::AA: $6*10^{-5}$ 1/s; DNA::TF::AA: 0.003 1/s.

Figure 4G: The expression rate settings to reflect the presence and the absence of synergy are the same as in **Figure 4E**. The binding rate constant of AA was set to 10^{-6} $s^{-1}molecule^{-1}$. The binding rate constant of the TF was scanned between 10^{-8} ... 10^{-5} $s^{-1}molecule^{-1}$ as plotted on the X axis.

Figure 4J: The binding rate constants of activators were set to 10^{-6} $s^{-1}molecule^{-1}$. The expression rates were set as follows: DNA::TF: $3*10^{-5}$ 1/s; DNA::AA: 0.003/[synergy] 1/s; DNA::TF::AA: 0.003 1/s. Synergy was varied between 1 and 100. For each synergy value, the "off" output was simulated by setting the expression rate of TF to $3*10^{-6}$ 1/s (representing low leakage) and the "on" level was simulated by setting the expression rate of TF to $3*10^{-3}$ 1/s. The On, Off and the On:Off values are plotted.

Supplemental References

Bleris L, Xie Z, Glass D, Adadey A, Sontag E, Benenson Y (2011) Synthetic incoherent feedforward circuits show adaptation to the amount of their genetic template. *Molecular Systems Biology* **7**

Boss V, Talpade DJ, Murphy TJ (1996) Induction of NFAT-mediated transcription by Gq-coupled receptors in lymphoid and non-lymphoid cells. *The Journal of biological chemistry* **271:** 10429-10432

Buckley SMK, Delhove JMKM, Perocheau DP, Karda R, Rahim AA, Howe SJ, Ward NJ, Birrell MA, Belvisi MG, Arbuthnot P, Johnson MR, Waddington SN, McKay TR (2015) In vivo bioimaging with tissue-specific transcription factor activated luciferase reporters. *Sci Rep-Uk* **5**

Chen Z, Manley JL (2003) Core promoter elements and TAFs contribute to the diversity of transcriptional activation in vertebrates. *Molecular and cellular biology* **23:** 7350-7362

Fang B, Mane-Padros D, Bolotin E, Jiang T, Sladek FM (2012) Identification of a binding motif specific to HNF4 by comparative analysis of multiple nuclear receptors. *Nucleic Acids Research* **40:** 5343-5356

Fiering S, Northrop JP, Nolan GP, Mattila PS, Crabtree GR, Herzenberg LA (1990) Single Cell Assay of a Transcription Factor Reveals a Threshold in Transcription Activated by Signals Emanating from the T-Cell Antigen Receptor. *Gene Dev* **4:** 1823-1834

Huang Q, Gong C, Li J, Zhuo Z, Chen Y, Wang J, Hua ZC (2012) Distance and helical phase dependence of synergistic transcription activation in cis-regulatory module. *PloS one* **7:** e31198

Kuhlbrodt K, Herbarth B, Sock E, Hermans-Borgmeyer I, Wegner M (1998) Sox10, a novel transcriptional modulator in glial cells. *The Journal of neuroscience : the official journal of the Society for Neuroscience* **18:** 237-250

Lagrange T, Kapanidis AN, Tang H, Reinberg D, Ebright RH (1998) New core promoter element in RNA polymerase II-dependent transcription: sequence-specific DNA binding by transcription factor IIB. *Genes & development* **12:** 34-44

Lapique N, Benenson Y (2014) Digital switching in a biosensor circuit via programmable timing of gene availability. *Nature Chemical Biology* **10:** 1020-1027

Larsson E, Lindahl P, Mostad P (2007) HeliCis: a DNA motif discovery tool for colocalized motif pairs with periodic spacing. *BMC bioinformatics* **8:** 418

Leisner M, Bleris L, Lohmueller J, Xie Z, Benenson Y (2010) Rationally designed logic integration of regulatory signals in mammalian cells. *Nature Nanotechnology* **5:** 666-670

Li QF, Wang XR, Yang YW, Lin H (2006) Hypoxia upregulates hypoxia inducible factor (HIF)-3alpha expression in lung epithelial cells: characterization and comparison with HIF-1alpha. *Cell research* **16:** 548-558

Peirano RI, Wegner M (2000) The glial transcription factor Sox10 binds to DNA both as monomer and dimer with different functional consequences. *Nucleic Acids Res* **28:** 3047-3055

Prochazka L, Angelici B, Haefliger B, Benenson Y (2014) Highly modular bow-tie gene circuits with programmable dynamic behaviour. *Nature communications* **5**

Schodel J, Oikonomopoulos S, Ragoussis J, Pugh CW, Ratcliffe PJ, Mole DR (2011) High-resolution genome-wide mapping of HIF-binding sites by ChIP-seq. *Blood* **117:** E207-E217

Senkel S, Lucas B, Klein-Hitpass L, Ryffel GU (2005) Identification of target genes of the transcription factor HNF1beta and HNF1alpha in a human embryonic kidney cell line. *Biochimica et biophysica acta* **1731:** 179-190

Takagi H, King GL, Ferrara N, Aiello LP (1996) Hypoxia regulates vascular endothelial growth factor receptor KDR/Flk gene expression through adenosine A(2) receptors in retinal capillary endothelial cells. *Invest Ophth Vis Sci* **37:** 1311-1321

Takagi S, Nakajima M, Kida K, Yamaura Y, Fukami T, Yokoi T (2010) MicroRNAs regulate human hepatocyte nuclear factor 4alpha, modulating the expression of metabolic enzymes and cell cycle. *The Journal of biological chemistry* **285:** 4415-4422

Tronche F, Ringeisen F, Blumenfeld M, Yaniv M, Pontoglio M (1997a) Analysis of the distribution of binding sites for a tissue-specific transcription factor in the vertebrate genome. *Journal of molecular biology* **266:** 231-245

Tronche F, Ringeisen F, Blumenfeld M, Yaniv M, Pontoglio M (1997b) Analysis of the distribution of binding sites for a tissue-specific transcription factor in the vertebrate genome. *Journal of Molecular Biology* **266:** 231-245

Veeman MT, Slusarski DC, Kaykas A, Louie SH, Moon RT (2003) Zebrafish prickle, a modulator of noncanonical Wnt/Fz signaling, regulates gastrulation movements. *Curr Biol* **13:** 680-685

Weber W, Kramer BP, Fux C, Keller B, Fussenegger M (2002) Novel promoter/transactivator configurations for macrolide- and streptogramin-responsive transgene expression in mammalian cells. *The journal of gene medicine* **4:** 676-686

Wolner BS, Gralla JD (2000) Roles for non-TATA core promoter sequences in transcription and factor binding. *Molecular and cellular biology* **20:** 3608-3615

Wu G, Bohn S, Ryffel GU (2004) The HNF1beta transcription factor has several domains involved in nephrogenesis and partially rescues Pax8/lim1-induced kidney malformations. *European journal of biochemistry / FEBS* **271:** 3715-3728